Physics – Uspekhi **51** (8) 793 – 814 (2008)

REVIEWS OF TOPICAL PROBLEMS PACS numbers: 41.75.Jv, **52.38.–r**, 79.20.Ds

Generation of fast charged particles and superstrong magnetic fields in the interaction of ultrashort high-intensity laser pulses with solid targets

V S Belyaev, V P Krainov, V S Lisitsa, A P Matafonov

DOI: 10.1070/PU2008v051n08ABEH006541

Contents

Abstract. Recent experimental and theoretical investigations are reviewed concerning the generation of fast charged particles and superstrong magnetic fields in the interaction of ultrashort laser pulses with solid targets. The mechanisms of generating fast charged particles in superstrong light fields of laser radiation with intensities ranging from 10^{17} to 10^{21} W cm^{-2} are considered. Electron acceleration due to vacuum heating, the ponderomotive potential, resonance absorption, the laser-driven wake field in the underdense part of plasma, cyclotron mechanism and some other mechanisms are thoroughly analyzed. Experimental data on the acceleration of protons and atomic ions by spatial charge fields on thin and thick solid targets are presented and theoretically interpreted. Particular attention is paid to the generation of superstrong quasistatic magnetic fields in laser plasmas and methods for measuring them under the action of various laser pulses of both femto- and picosecond durations. The possible formation of magnetic plasma configurations and magnetic plasma confinement are discussed.

V S Belyaev, A P Matafonov
Central Research Institute of Machine Building,
Pionerskaya ul. 4, 141070 Korolev, Moscow region, Russian Federation
Tel. (7-495) 513 54 44
E-mail: vadimbelyaev@mtu-net.ru
V P Krainov Moscow Institute of Physics and Technology,
Institutskii per. 9, 141700 Dolgoprudnyi, Moscow region,
Russian Federation
Tel. (7-495) 408 75 90. Fax (7-495) 408 68 69
E-mail: vpkrainov@mail.ru
V S Lisitsa Nuclear Fusion Institute, Russian Research Centre
'Kurchatov Institute',
pl. Kurchatova 1, 123182 Moscow, Russian Federation
Tel. (7-499) 196 73 34. Fax (7-495) 943 00 73
E-mail: lisitsa@nfi.kiae.ru

Received 26 December 2007, revised 26 March 2008
Uspekhi Fizicheskikh Nauk **178** (8) 823 – 847 (2008)
DOI: 10.3367/UFNr.0178.200808b.0823
Translated by N A Raspopov; edited by A Radzig

1. Introduction

The development of a new generation of solid-state lasers has resulted in unique conditions for irradiating laser targets by light pulses, with radiation intensity ranging from 10^{17} to 10^{21} W cm^{-2} and a duration of 20 – 1000 fs.

At such intensities, the laser pulse produces superstrong electric fields which could not be obtained earlier and considerably exceed the atomic electric field of strength $E_a = 5.14 \times 10^9$ V cm^{-1}. In these conditions, there arises a new physical picture of laser pulse interaction with plasma produced when the pulse leading edge or a pre-pulse affects solid targets. Laser radiation is rather efficiently transformed into fluxes of fast charged particles such as electrons and atomic ions. The latter interact with the ambient material of the target, which leads to the generation of hard X-rays, when inner atomic shells are ionized, and to various nuclear and photonuclear reactions.

One important area in investigating the interaction of subpicosecond laser pulses with solid targets is related to the important role which arising superstrong quasistatic magnetic fields and electronic structures play in laser plasma dynamics. This area of research became most attractive after carrying out the direct measurements of quasistatic magnetic fields on the Vulcan laser system (Great Britain) [1], in particular, after the pinch effect has been found experimentally in laser plasma [2].

The relativistic character of laser radiation with intensity I is realized at the magnitude of a dimensionless parameter $a > 1$. This parameter represents the dimensionless momen-

tum of the electron oscillating in the electric field of linearly polarized laser radiation and can be expressed as

$$a = \frac{eE}{mc\omega} = 0.85\,\lambda\left(\frac{I}{10^{18}}\right)^{1/2}, \tag{1}$$

$$E = 27.7\,I^{1/2}, \tag{2}$$

where e and m are the charge and mass of the electron, respectively, E is the amplitude of electric field strength (in units of V cm^{-1}) of laser radiation, λ is the radiation wavelength (in μm), ω is the frequency of laser radiation, c is the speed of light, and I is the radiation intensity (in W cm^{-2}).

Terawatt-power laser systems of moderate size can fulfill the condition $a > 1$, which corresponds to the electric field strength above 10^{10} V cm^{-1}. In such intense fields, the over-barrier ionization of atoms occurs in atomic time on the order of 10^{-17} s, and the electrons produced are accelerated and reach MeV-range relativistic energies during the laser pulse.

The acceleration of atomic ions in femto- and picosecond laser plasmas constitutes a secondary process. It is caused by the strong quasistatic electric fields arising due to spatial charge separation. Such separation is related to the motion of a bunch of fast electrons. For laser radiation intensities exceeding $I \geqslant 10^{18}$ W cm^{-2}, it is possible to obtain directed beams of high-energy ions with the energies $\varepsilon_i > 1$ MeV.

The generation of high-energy proton and ion beams in laser plasma under the action of ultrashort pulses is a quickly developing field of investigations. This is explained, in particular, by their important applications in such fields as proton accelerators, the study of material structure, proton radiography, the production of short-living radioisotopes for medical purposes, and laser controlled fusion [3, 4]. For a laser radiation intensity of $I \geqslant 10^{18}$ W cm^{-2}, a number of nuclear reactions can be initiated that have only been realized in elementary particle accelerators [5].

Later on, we will consider the principal mechanisms for generating fast charged particles and quasistatic magnetic fields in laser plasmas, as well as experimental results obtained both abroad and on the native laser setup NEODIM in the Central Research Institute of Machine Building (*Russ. abbr.* TsNIIMash) (Korolev, Moscow reg.) [6, 7]. The review is mainly devoted to the experimental and theoretical results obtained in recent years with particular attention focused on simple physical models of the processes considered. Earlier results were sufficiently well considered in reviews [3 – 5]. In those works, the theory was based on calculations performed with large modern computers by using particle-in-cell methods and the classical dynamics of particles.

2. Generation of fast electrons in laser plasma

In irradiating a target by a high-intensity ultrashort laser pulse, the radiation energy is rather efficiently converted into the energy of fast electrons which later partially transfer their energy to the atomic ions of the target. Presently, several mechanisms are being discussed concerning the generation of fast electrons when a laser pulse affects plasma with a density well above the critical value. If the laser pulse is not accompanied by a pre-pulse (the case of high contrast), then the laser radiation interacts with plasma of a solid-state density, possessing a sharp boundary. In this case, the mechanism of 'vacuum heating' is realized [8], as is the so-called $\mathbf{v} \times \mathbf{B}$ mechanism [9] (here, $\mathbf{B}$ is the magnetic field induction of the laser field) caused by a longitudinal ponderomotive force acting along the propagation direction of the laser pulse). This $\mathbf{v} \times \mathbf{B}$ mechanism becomes substantial at relativistic intensities where the energy of electron oscillations is comparable with or exceeds the electron rest energy $mc^2 = 511$ keV — that is, for the parameter $a > 1$ [see formula (1)]. In addition, fast electrons can be generated on the critical surface of plasma at a plasma resonance [10 – 12] if the vector of the laser radiation electric field has a projection along the density gradient (usually at an inclined incidence of laser radiation to target) and the laser frequency coincides with the plasma frequency. In contrast to the ponderomotive $\mathbf{v} \times \mathbf{B}$ mechanism, vacuum heating and resonance absorption arise at nonrelativistic (substantially lower, with $a < 1$) intensities as well. In the case of the ponderomotive mechanism, the average energy of fast electrons can be estimated as the maximum energy of transverse electron oscillations in an electromagnetic field, which in the general case takes a relativistic value. In a underdense part of the laser plasma, we have

$$\varepsilon_e = mc^2\left[\left(1 + \frac{Q}{Q_0}\right)^{1/2} - 1\right],$$
$$Q = I\lambda^2, \quad Q_0 = 1.37 \times 10^{18}\ \frac{\text{W}}{\text{cm}^2}\ \mu\text{m}^2. \tag{3}$$

In the ultrarelativistic limit $Q \gg Q_0$, we hence obtain

$$\varepsilon_e = mc^2\left(\frac{Q}{Q_0}\right)^{1/2}.$$

By contrast, in the nonrelativistic limit $Q \ll Q_0$, we derive from formula (3) that

$$\varepsilon_e = mc^2\,\frac{Q}{2Q_0}.$$

In the overdense part of the plasma, the ponderomotive heating of electrons is noticeably weaker due to a difficult penetration of the laser field into this region.

In the case of vacuum heating, the maximum energy of an electron flying into the depths of a dense target is given by the formula similar to Eqn (3), however, with a different numerical factor (see below).

There is one more mechanism for generating fast electrons in the underdense part of plasma in front of a target due to the betatron resonance in the arising magnetic field [13]. In this regime, electrons are accelerated by the transverse ultrarelativistic electric field of the laser wave in the direction of wave polarization, and the azimuthal magnetic field produced by the current of fast electrons is responsible for the magnetic part of the Lorentz force. This force turns electrons in such a way that they gradually change to the opposite direction of motion. In the case of an exact betatron resonance, the reflection occurs at the instant when the transverse electric field changes its direction, so the electrons are accelerated at all times. This mechanism yields an energy of fast electrons three times greater than formula (3) does:

$$\varepsilon_e = 3mc^2\left(\frac{Q}{Q_0}\right)^{1/2}. \tag{4}$$

There are also further mechanisms of electron acceleration that require special experimental conditions, for example, the wake field acceleration [14, 15]. In the case of resonance absorption, the electric field near the plasma

critical surface is much stronger than that of incident laser radiation. The result is that the heating of electrons upon their impact with atomic ions is greater than follows from formulae (3) and (4).

Electrons are also accelerated by a transverse ponderomotive force (acting in the radial direction) due to a focal distribution of laser intensity. This acceleration leads to the maximum electron energy also expressed by formula (3) (in the underdense part of plasma) if electrons succeed in acquiring this energy moving from the focus to the periphery during the laser pulse. Thus, the duration τ of a laser pulse should meet the inequality $\tau \gg m\omega R/eE$ (in the nonrelativistic case). Here, R is the radius of the focal spot of a laser beam. This inequality holds for picosecond- and longer-duration laser light pulses with an intensity on the order of 10^{16} W cm^{-2}. In fields with an intensity of 10^{18} W cm^{-2}, the right-hand side of this inequality reaches dozens of femtoseconds, whereas in the overdense part of plasma this ponderomotive force is noticeably weaker.

Following is discussion of the above-mentioned mechanisms in more detail.

2.1 Longitudinal ponderomotive acceleration of electrons in a skin layer

Let us consider the longitudinal ponderomotive acceleration of electrons under the action of a superstrong laser pulse falling onto the surface of a solid body, which is transformed to overdense plasma by the leading edge of the laser pulse. For definiteness, we limit our consideration to linearly polarized radiation with p-polarization, which is incident at a certain angle α with respect to the surface normal. Boundary conditions on the target surface and the known Fresnel formulae relating electromagnetic waves that are incident, reflected, and passed into a skin layer entail the following expressions for the tangential (E_t) and normal (E_n) projections of the electric field strength with exponential attenuation inside the skin layer (which hold for all values of α except for close to $\pi/2$):

$$E_t = i\,\frac{2\omega}{\omega_{pl}}\,E\exp(i\omega t - kz)\,,$$
$$E_n = -\frac{2\omega^2\sin\alpha}{\omega_{pl}^2}\,E\exp(i\omega t - kz)\,, \qquad (5)$$
$$k = \frac{\omega_{pl}}{c}\,.$$

Here, as in previous considerations, E and ω are the amplitude of electric field strength and the frequency of the incident laser wave, respectively, and ω_{pl} is the plasma frequency determined by the concentration n_e of free electrons:

$$\omega_{pl} = \sqrt{\frac{4\pi n_e e^2}{m}}$$

(m is the electron mass, and e is the elementary charge). Here, the z-coordinate is normally directed to the surface of the target into its depths. In deriving relationships (5) from the Fresnel formulae, we assumed that the permittivity of overdense plasma has the simple form (under realistic assumption that $\omega_{pl} \gg \omega$) determined by free electrons:

$$\varepsilon(\omega) = 1 - \frac{\omega_{pl}^2}{\omega^2} \approx -\frac{\omega_{pl}^2}{\omega^2}\,.$$

Hence $E_n \ll E_t \ll E$. The magnetic field intensity inside the skin layer (it has only the tangential component) is given by the relationship

$$B_t = 2E\exp(i\omega t - kz)\,. \qquad (6)$$

The longitudinal ponderomotive acceleration of electrons is produced by the magnetic (relativistic) part of the Lorentz force which acts on electrons in the skin layer. Let us calculate the force component that is normal to the target surface:

$$F_n = \frac{e}{c}\,\mathrm{Re}\,v_t\,\mathrm{Re}\,B_t\,. \qquad (7)$$

Here, v_t is the tangential component of electron velocity, which is normal to B_t. This velocity can be found from the equation for tangential motion of electrons taking into account only the electric part of the Lorentz force, because its magnetic part has no projection onto the tangential direction:

$$\frac{dp_t}{dt} = eE_t\,.$$

By inserting into this formula the tangential projection of the electric field strength inside the skin layer according to Eqn (5), we find the electron tangential momentum:

$$p_t = \frac{2e}{\omega_{pl}}\,E\exp(i\omega t - kz)\,. \qquad (8)$$

From relationships (6)–(8) we obtain (assuming for the sake of simplicity the tangential velocity to be small relative to the speed of light)

$$F_n = \frac{4e^2E^2}{mc\omega_{pl}}\exp(-2kz)\cos^2\omega t\,. \qquad (9)$$

For higher degree of relativity, this force grows linearly with the field strength E rather than quadratically, because

$$v_t = \frac{cp_t}{\sqrt{p_t^2 + m^2c^2}} \to c\,.$$

Averaging this force over the period of the laser wave yields

$$\overline{F_n} = \frac{2e^2E^2}{mc\omega_{pl}}\exp(-2kz)\,. \qquad (10)$$

This constant force acts inwards from the surface of the target regardless of the sign of the electric charge of the accelerated particle. It is of relativistic origin. For a higher degree of relativity, the longitudinal force changes, however, keeping the inward direction. In the ultrarelativistic limit we obtain from Eqn (7), instead of formula (9), the expression

$$F_n = 2eE\exp(-kz)\left|\cos\omega t\right|.$$

Expressions (9) and (10) can also be obtained in a different way that stresses the character of F_n as a longitudinal *ponderomotive* force in a spatially inhomogeneous laser field. The energy of electron vibrations in a skin layer is determined by its tangential motion, since the tangential velocity is high relative to the normal velocity (see the comparison between the tangential and normal components of electric field

strength given above). Thus, using formula (8) we obtain the expression for this energy:

$$\varepsilon_e = \frac{m(\mathrm{Re}\, v_t)^2}{2} = \frac{2e^2E^2}{m\omega_{pl}^2} \exp(-2kz) \cos^2 \omega t .$$

The gradient of this energy, $-\mathrm{d}\varepsilon_e/\mathrm{d}z$, yields the expression for the longitudinal ponderomotive force, which coincides with formula (9) if one takes into account that $k = \omega_{pl}/c$. This longitudinal force leads to the longitudinal drift of electrons with a constant velocity inward from the target surface.

The average energy of the longitudinal drift, acquired by an electron over the period of the laser wave, is given by

$$\varepsilon_e = \frac{e^2E^2}{m\omega_{pl}^2} \exp(-2kz) .$$

An electron acquires the maximum kinetic energy when it resides on the surface of the target:

$$\varepsilon_e = \frac{e^2E^2}{m\omega_{pl}^2} .$$

This energy is independent of the angle α at which the laser radiation is incident on the target. It is considerably lower than energy (3) acquired by an electron in a transverse (radial) direction in the underdense part of the plasma if we are dealing with picosecond or longer-duration pulses.

In the ultrarelativistic limit, the maximum electron energy becomes linear in the field, because the $\mathbf{v} \times \mathbf{B}$-force, as was shown, is linear in the field strength. One can estimate the ultrarelativistic longitudinal energy in this case as follows:

$$\varepsilon_e \propto \frac{eEc}{\omega_{pl}} . \qquad (11)$$

It should be noted that the transverse ponderomotive force in the skin layer is determined by the gradient of energy ε_e with respect to the radius R of the focus spot. It is small compared to the longitudinal ponderomotive force under the condition that the depth c/ω_{pl} of the skin layer is small relative to R. This condition often holds because the radius of the focus spot is usually 5–15 μm, whereas the depth of a skin layer is only 100–300 Å. However, the transverse ponderomotive energy determined in the general relativistic case by relationship (3) exceeds the longitudinal ponderomotive energy (8), since, for example, in the nonrelativistic limit it comprises the frequency ω of laser radiation in the denominator instead of plasma frequency ω_{pl}. At high kinetic energies of electrons, the conversion of the longitudinal energy into transverse energy and vice versa is hindered by the absence of impacts between electrons and atomic ions.

The above-performed averaging of the energy and force over the period of the laser wave is reasonable under the condition that the time of passing through the skin layer is long compared to the light wave period. The condition reduces to the moderate relativity constraint

$$\frac{eE}{mc\omega} < 1 .$$

In the opposite case, one can apply formula (11) for estimating the relativistic energy of an electron.

Finally, note that the transverse ponderomotive force, which is radially directed, pushes a portion of the electrons from the axis of a laser beam to its periphery. This results in the plasma frequency reducing on the channel axis and becoming closer to the laser frequency. This reduction is more pronounced at relativistic intensities and increases the depth of the skin layer (the so-called relativistic blooming of laser plasma). The resulting relativistic longitudinal ponderomotive energy (11) increases to a value on the order of the transverse relativistic ponderomotive energy (3).

2.2 Vacuum heating

In the above consideration we did not take into account that electrons may escape back to a vacuum under the action of the normal component of the electric field inside a skin layer (of course, only when a nonrelativistic laser pulse with p-polarization is inclined with respect to the target). After a fraction of the laser period, the electron may reverse its direction of motion due to the alternative character of the laser field (depending on its phase at the instant of electron escape) and hit the target with an average energy on the order of its transverse ponderomotive energy. The numerical nonrelativistic simulation performed in Ref. [8] yields the following value for the electron energy (on laser beam incidence at angle α with the normal to the target surface):

$$\varepsilon_e = 0.78 \frac{e^2E^2}{m\omega^2} \sin^2 \alpha . \qquad (12)$$

The numerical factor in this formula (on the order of unity) is determined by averaging over the phase of the instant of the electron escape from the target surface relative to the phase of laser field. It is also determined by a retarding action of the bunch of electrons that escaped the target earlier. Electron energy (12) is large compared to that obtained from the longitudinal ponderomotive heating, because $\omega^2 \ll \omega_{pl}^2$. Thus, the longitudinal ponderomotive heating of electrons in the skin layer is weaker than the vacuum heating (if one neglects the above-mentioned relativistic blooming of the target on the axis of the laser beam).

Nevertheless, the mechanism of vacuum heating implies the sharp transfer from the vacuum to the overdense plasma. Actually, the electron concentration gradually falls near the critical surface where the laser radiation frequency is equal to the plasma frequency. Correspondingly, the energy acquired by the electrons reduces with decreasing gradient of electron concentration in plasma compared to that given by expression (12). On the one hand, it follows from the equation of motion that the velocity acquired by the electrons at a small concentration gradient is proportional to the gradient. On the other hand, the laser field penetrates more deeply into the overdense region at the gradual concentration gradient near the critical surface, and more electrons are involved in the process of vacuum heating.

From the above consideration it is obvious that realization of vacuum heating requires a high contrast of the laser pulse. Remember that expression (12) was first obtained by Brunel [8] in the nonrelativistic approximation.

One should take into account that a focused laser beam in the underdense part of a plasma induces, according to the Maxwell equations, the longitudinal oscillating electric field with the amplitude being lesser than the transverse field amplitude by a factor of $\omega R/c$ (here, R is the radius of the focus spot) [16]. Its direct contribution to electron acceleration is small due to the oscillating character of this field and because the condition $\omega Rc \gg 1$ usually holds, although the longitudinal electric field enhances the vacuum heating.

In the underdense part of a plasma, electrons may also acquire kinetic energy in collisions with atomic ions in the presence of a laser field (stimulated inverse bremsstrahlung). In a collision with an atomic ion, an electron can either absorb a laser photon or emit it. However, the probability of absorbing the photon is somewhat higher than the probability of emitting it. The average energy acquired in a single impact is equal (in a linearly polarized field) to the double ponderomotive energy:

$$\varepsilon_e = \frac{e^2 E^2}{2m\omega^2} . \qquad (13)$$

Although this energy is comparable to that obtained in vacuum heating, the real contribution from this mechanism is small due to the low concentration of electrons and ions in the underdense part of the plasma.

In paper [17], the generation of hot electrons was studied in the interactions of *p*-polarized laser pulses possessing a 150-fs duration, a peak intensity of 8×10^{15} W cm^{-2}, and a wavelength of 800 nm with various solid targets. The contrast of laser radiation amounted to 10^5. The experiment showed that it is exactly the vacuum mechanism that is the main mechanism for heating hot electrons. From formula (12), the temperature of hot electrons was found to be 50 keV.

In theoretical work [18], the authors generalizing the mechanism of vacuum heating to the relativistic case noticed that the leading edge of the returning electrons moves more slowly than the trailing edge. Hence, the hydrodynamic stall of the electron bunch may occur, which results in collisions between electrons, their stochastic motion, and the stochastic heating of plasma.

Then, the electrons heated in the process of stimulated inverse bremsstrahlung in the underdense part of the plasma may traverse the skin layer in a time shorter than the period of the laser wave (nonadiabatically). At a skin layer depth of 200 Å, this occurs at an electron kinetic energy above 200 eV. This case was considered in recent work [19]. It was shown that in these conditions the absorption in the underdense part of the plasma dominates that in the skin layer due to the vacuum heating mechanism. It is especially revealed at relativistic intensities above 10^{19} W cm^{-2}. However, the vacuum mechanism is only valid for electrons which reside in the overdense region near the plasma critical surface — this is the only place from which electrons may be extracted by the laser field of the incident wave to the underdense region. The situation is hindered by the fact that an electron in the underdense region is affected by both the incident and reflected laser waves and its motion transfers from oscillating to stochastic mode. The stochastic variant of vacuum heating was thoroughly considered in Refs [20, 21].

In recent experiment [22], electrons with an energy above 300 MeV were detected in circumstances where the interaction between plasma and laser radiation with an intensity exceeding 3×10^{20} W cm^{-2} occurred (Fig. 1). At the leading edge of the laser pulse, a superhigh-power laser throws out all plasma electrons in radial directions from the focal space by a transverse ponderomotive force. In the process, a purely ion channel is produced, through which the main part of the superhigh-power laser pulse passes freely. The Coulomb field of positive ions, which propagates at almost the speed of light (the ions themselves are, of course, at rest), draws electrons, accelerating them to ultrarelativistic energies. The flux of electrons moving along the laser beam produces a strong

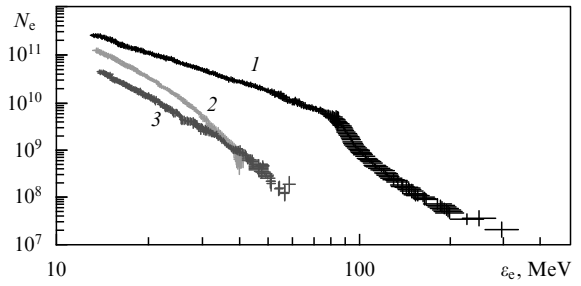

Figure 1. Electron spectra taken at various electron densities: *1* — $n_e = 7.7 \times 10^{18}$ cm^{-3}, *2* — $n_e = 83 \times 10^{18}$ cm^{-3}, and *3* — $n_e = 5.4 \times 10^{18}$ cm^{-3} (N_e is the number of electrons per MeV per sr).

circular quasistatic magnetic field. The field is detected experimentally as well. Then, the focus spot enlarges due to diffraction, which reduces the transverse ponderomotive force and weakens the effect of the relativistic blooming of the channel.

In work [23], a relativistic laser pulse is normally incident on a solid target and vacuum heating occurs due to the magnetic part of the Lorentz force, because the electric part makes no contribution.

Electrons residing in the underdense part of the plasma cannot be directly accelerated by the laser pulse, because the adiabatic acceleration at the leading edge of the laser pulse is replaced by similar adiabatic deceleration at its trailing edge. In paper [24], it was suggested to place a separator from dense plasma (thin foil), which would block the laser field and act as a nonadiabatic factor, so that the accelerated electrons would traverse the separator prior to the deceleration starting. The corresponding calculations for the motion of an accelerated electron were given in Ref. [25]. In accelerating electrons by a strongly focused laser beam, the main role in the process is played by the longitudinal electric field mentioned above. In the field with intensity of 10^{19} W cm^{-2}, the energy of such accelerated electrons is above several MeV [26].

As noted above, the transverse ponderomotive force pushes electrons out of a focus zone of the strong traveling laser wave to the periphery. Interestingly, in the case of a standing relativistic laser wave (for example, in the region close to the plasma critical surface because of strong reflection of the wave), an electron, on the contrary, is mainly drawn in to the region with a stronger field [27] rather than pushed out by the field, although at short distances its motion is stochastic in character.

In paper [28], the influence of laser beam polarization on the magnitude of the ponderomotive force in a underdense part of plasma was considered. It was shown that the circular field results in a stronger ponderomotive force than the linearly polarized field does (at the same radiation power). This fact was confirmed by numerical simulations [29].

One can imagine the motion of electrons in a skin layer as the longitudinal motion of the electron bunch with the lateral dimension far greater than the longitudinal one. For example, according to the calculations performed in Ref. [30] by the particle-in-cell technique at the laser pulse intensity on the order of 10^{20} W cm^{-2} and a wavelength of 1 μm, the lateral dimension of the bunch is on the order of 350 μm, whereas the longitudinal dimension amounts only to 20 μm. Thus, the electron bunch constitutes a thin disk moving inward from the target surface normally to the disk's plane. The average

energy of an ultrarelativistic electron in such a bunch is about 60 MeV.

In the framework of quasistationary approximation [31], plasmic-field structures were considered that arise in circumstances where the interaction of a relativistically strong electromagnetic wave with the layer of an overdense plasma occurs. It was shown that at the incident field amplitudes exceeding a certain threshold value, in addition to conventional solutions which are nonlinear generalizations of skin-layer solutions, the multilayer structures may be excited that incorporate cavitation zones from which all electrons are completely pushed out (ion layers). In such cavitation zones which function as self-consistent cavities, the field may be amplified and the corresponding electromagnetic energy may be stored.

Longitudinal motion of electrons along the laser beam only occurs in the central part of the channel. At the periphery, free electrons move in the opposite direction. The electron reverse current is explained by the fact that electrons are no longer affected by the longitudinal ponderomotive force; the intention to compensate for the direct current follows from the Le Chatelier principle. The reverse current can also be explained in the following way: the electron direct current produces a circular magnetic field on the periphery of the laser focus. This magnetic field affects peripheral electrons moving in the transverse radial direction outward from the channel axis under the action of a transverse ponderomotive force. Just the magnetic part of the Lorentz force originates the reverse flow of peripheral electrons.

In paper [32], the authors analyzed the efficiency of electron acceleration by the ponderomotive force that arises when high-intensity laser pulses interact with plasma. The force acting on an electron may be rather strong: up to 1 GeV cm^{-1}. The theoretical predictions were verified by the tests conducted with the help of 2D particle-in-cell simulation.

2.3 Resonance absorption of laser radiation

Let us consider now one more mechanism of electron heating by laser radiation. It is based on resonance laser excitation of plasma oscillations in the solid target, in which the laser pulse frequency ω is close to the plasma frequency $\omega_{\rm pl} = \sqrt{2\pi n_{\rm e}}$ (in this section we use the Hartree atomic system of units: $\hbar = e = m_{\rm e} = 1$) of 3D vibrations of the electron bunch near the surface of the irradiated solid body. After the ionization, the plasma frequency inside the solid body is, of course, several times the frequency of a typical laser (for example, an Nd:glass or Ti:sapphire laser). Here, we consider a less-dense laser plasma (pre-plasma) mainly produced by a laser pre-pulse near the body surface. This plasma expands relatively slowly (at the ion sound velocity) from the irradiated target towards the laser radiation, with the electron concentration in the plasma varying from zero to the overdense value in the skin layer of the target.

We may calculate the energy absorbed by a unit of volume of pre-plasma per unit time. It is given by the general electrodynamic relationship

$$\frac{\partial U}{\partial t} = \frac{1}{4\pi}\, E(t)\, \frac{\partial D(t)}{\partial t}\,. \tag{14}$$

Here, the following notation was introduced:

$$E(t) = \frac{1}{2}\left[E\exp\left(\mathrm{i}\omega t\right) + E^{*}\exp\left(-\mathrm{i}\omega t\right)\right]$$

is the electric field strength (for simplicity we assume that the field is linearly polarized) inside plasma, and

$$D(t) = \frac{1}{2}\left[E\varepsilon(\omega)\exp\left(\mathrm{i}\omega t\right) + E^{*}\varepsilon^{*}(\omega)\exp\left(-\mathrm{i}\omega t\right)\right]$$

is the electric field induction, with $\varepsilon(\omega)$ being the complex permittivity. Averaging over the laser pulse period yields

$$\frac{\partial U}{\partial t} = \frac{\omega}{8\pi}\,\mathrm{Im}\,\varepsilon(\omega)|\,E\,|^{2}\,. \tag{15}$$

The complex electric field E inside plasma is related to the field E_0 of the incident electromagnetic wave in a vacuum through boundary conditions. For definiteness, we consider the case of a laser pulse incident on the surface of a solid target at an angle of 45°; notice that resonance absorption is absent for normal incidence of the laser pulse on a target surface. Near resonance, the component of the electric field which is normal to the target surface is large compared to the tangential one due to small permittivity, hence we may neglect the tangential component. In the simplified statement of the problem, we assume a sharp boundary between the vacuum and plasma with the plasma frequency close to the resonance frequency (i.e., the critical surface). Then, the boundary condition of continuity for the normal projection of electric field induction entails the following expression for the normal component of the electric field intensity inside the target:

$$E = \frac{1}{\varepsilon(\omega)\sqrt{2}}\,E_0\,. \tag{16}$$

In the Drude model, the permittivity due to free plasma electrons has the simple form

$$\varepsilon(\omega) = 1 - \frac{\omega_{\rm pl}^{2}}{\omega(\omega + \mathrm{i}\nu_{\rm ei})} \approx 1 - \left(\frac{\omega_{\rm pl}}{\omega}\right)^{2} + \mathrm{i}\,\frac{\omega_{\rm pl}^{2}\nu_{\rm ei}}{\omega^{3}}\,, \tag{17}$$

where $\nu_{\rm ei} \ll \omega$ is the frequency of electron – ion collisions. The latter is given by the Spitzer relationship [33]

$$\nu_{\rm ei} = \frac{4\sqrt{2\pi}\,Zn_{\rm e}}{3T_{\rm e}^{3/2}}\,\ln\Lambda\,, \tag{18}$$

where Z is the charge of atomic ions in plasma, $T_{\rm e}$ is the electron temperature, and $\ln\Lambda$ is the standard Coulomb logarithm. It follows from formula (16) that the electric field dramatically strengthens at resonance compared to that of the incident laser radiation.

By substituting the obtained values we may write out the following expression for the power absorbed in a unit of plasma volume near resonance $\omega = \omega_{\rm pl}$:

$$\frac{\partial U}{\partial t} = \frac{E_0^{2}}{16\pi}\,\frac{\omega^{4}\nu_{\rm ei}}{\left(\omega_{\rm pl}^{2} - \omega^{2}\right)^{2} + \left(\omega\nu_{\rm ei}\right)^{2}}\,. \tag{19}$$

In particular, the exact resonance $\omega = \omega_{\rm pl}$ entails

$$\frac{\partial U}{\partial t} = \frac{3E_0^{2}T_{\rm e}^{3/2}}{16\sqrt{2\pi}\,Z\ln\Lambda}\,. \tag{20}$$

As noted above, the average energy absorbed by an electron when it collides with an atomic ion in the presence of a laser field is twice the field ponderomotive energy $\varepsilon_{\rm e} = E^{2}/2\omega^{2}$. The following collision is hindered by the high energy acquired by the electron in the first collision. Hence, we may take into account only the first electron collision with an atomic ion. Thus, we obtain the following relationship for

the temperature T_e included in the above formulae (for the exact resonance):

$$T_e = \frac{2}{3}\,\varepsilon_e = \frac{E^2}{3\omega^2} = \frac{E_0^2}{6\nu_{ei}^2}\,.$$

Hence, at exact resonance we find

$$T_e = \frac{2Z\ln\Lambda\omega_{pl}^2}{3\sqrt{\pi}E_0}\,. \tag{21}$$

By inserting formula (21) into equation (20) we can finally write out (in atomic units)

$$\frac{\partial U}{\partial t} = \frac{\omega\sqrt{ZE_0\ln\Lambda}}{8\pi^2}\,. \tag{22}$$

Resonance absorption, of course, increases with the growth in electric field intensity, but is merely proportional to the square root of the intensity.

In fact, the resonance absorption is determined by the rate of electron concentration change near the critical surface. If it is sufficiently high, then the resonance region is small and plasma quickly leaves the resonance region as a laser pulse passes through it. This case corresponds to the absence of a pre-pulse and to an ultrashort laser pulse duration. Here, vacuum heating dominates, which was considered above. Conversely, the resonance absorption is substantial at a longer duration of the laser pulse and a greater dimension of the pre-plasma region produced by both the leading edge of the laser pulse and various pre-pulses. In accordance with formula (19), the condition of recovering from resonance has the form

$$\omega_{pl}^2 - \omega^2 = 4\pi\left[n_e(0) - n_e(z)\right] \sim \omega\nu_{ei}\,.$$

By presenting the electron concentration near the critical surface in the form

$$n_e(z) = n_e(0) + \frac{dn_e}{dz}\,z\,,$$

we obtain the estimate for the depth z of the region in which the resonance absorption occurs:

$$z \sim \frac{\omega\nu_{ei}}{4\pi}\left(\frac{dn_e}{dz}\right)^{-1}.$$

Multiplying this expression by Eqn (19) and by the area πR^2 of the focus spot we find the power absorbed on the critical surface:

$$W \approx \frac{E_0^2R^2\omega^3}{128\pi}\left(\frac{dn_e}{dz}\right)^{-1}. \tag{23}$$

This expression is more general than the previous formulae, because it does not comprise the electron–ion collision frequency. Thus, it holds for each mechanism that determines the width of plasma resonance.

Let us next estimate the fraction of the laser pulse energy absorbed in the conditions of resonance absorption. The incident power is determined by the Poynting vector (again, with a 45° angle of incidence)

$$W_0 = \frac{cE_0^2}{16\pi}\,\pi R^2\,.$$

By dividing Eqn (23) by this expression we arrive at (in atomic units)

$$\frac{W}{W_0} = \frac{\omega^3}{8\pi c}\left(\frac{dn_e}{dz}\right)^{-1}.$$

The radiation intensity and radius of the focal spot are not included in this expression. Since in atomic units $c = 137$ and the typical laser frequency is 1/20 a.u., we find the estimate $z \sim 2c/\omega \sim 0.3$ μm for the characteristic depth of pre-plasma, in which the critical electron concentration should be maintained constant in order to provide the absorption of a sufficient part of the laser energy on the critical surface.

2.4 Cyclotron mechanism of electron acceleration

The magnetic activity of picosecond laser plasma offers new mechanisms for the generation of fast electrons due to the presence of such strong quasistatic magnetic fields regardless of the mechanisms of their origin. Such a possibility is related to the emergence of cyclotron resonances when the laser frequency ω coincides with the Larmor gyration frequency $\Omega = eB_0/m_rc$ of an electron in an external constant magnetic field with the induction B_0 (here, e and m_r are the charge and relativistic mass of the electron, respectively; c is the speed of light). Indeed, the typical laser frequency ω is on the order of 0.05 a.u. and coincides with the cyclotron frequency at an induction of $B_0 = 7$ a.u. ~ 100 MG. This value may become much greater with allowance made for the relativistic increase in electron mass, which is typical at laser radiation intensities on the order of $10^{19} - 10^{20}$ W cm^{-2}. Hence, the generation of a constant magnetic field results in stronger interaction of laser radiation with plasma. The situation is to a certain extent similar to the radiation self-focusing effect, in which case the variations in the refraction index of the medium in the field of a laser wave influence wave propagation through the medium.

In the general relativistic case, the interaction of electrons with the field of a laser wave and with the constant magnetic field $\mathbf{B}_0$ is written out in the form

$$\frac{d\mathbf{p}}{dt} = e\left\{\mathbf{E} + \frac{1}{c}\,\mathbf{v}\times(\mathbf{B}+\mathbf{B}_0)\right\} \tag{24}$$

for electrons possessing a momentum $\mathbf{p}$ and a velocity $\mathbf{v}$.

For circular polarization, the problem is solved analytically, whereas in the general case of linear polarization the problem reduces to a system of nonlinear equations, which can only be solved numerically. The solution to these equations is specific in that there are resonances between the periodic motion of electrons in the magnetic field and electron oscillations in the field of the laser wave. This fact leads to drastic changes in electron trajectory and energy at certain instants of time.

Figure 2 depicts the variations in the kinetic energy of an electron (a) and its trajectory (b) for motion with the zero initial velocity in a field with a radiation intensity of 10^{20} W cm^{-2} and a frequency that is at resonance with the cyclotron frequency [34]. The constant magnetic field is normal to the polarization of laser radiation. One can see that an electron acquires an energy of approximately 100 MeV in a time on the order of hundreds of femtoseconds.

Electron acceleration in the field of a circularly polarized laser wave propagating along a strong magnetic field was theoretically investigated in lectures [35]. It was shown that

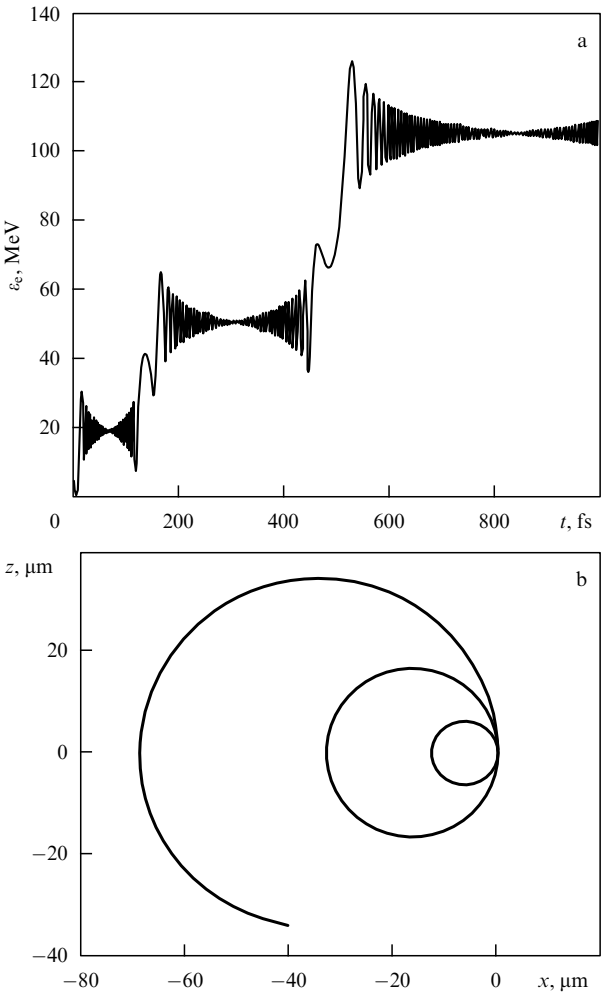

Figure 2. Electron kinetic energy (a) and trajectory (b) in a linearly polarized laser wave with an intensity of 10^{20} W cm^{-2} and a constant transverse magnetic field in the resonance case of $\Omega = \omega$.

the relativistic factor of the electron may increase by an order of magnitude under a high intensity of laser radiation.

2.5 Wake-field electron acceleration in underdense plasma

Let us consider here one more mechanism of electron acceleration. In the underdense part of laser plasma produced by pre-pulses, when a high-power laser pulse is incident on the surface of a solid body, the later passing main part of the laser pulse induces longitudinal plasma oscillations. The energy is transferred from the laser pulse to the plasma wave in the following way. The longitudinal ponderomotive force draws electrons out in the direction of the laser pulse, and a positive charge arises at the site where the electrons resided. Thus, temporal charge separation is observed. The expelled electrons are attracted to stationary positive ions by Coulomb forces and start moving back. Thus, longitudinal plasma waves arise in the underdense part of the plasma, which follow the laser pulse. Their phase velocity matches the group velocity of the laser wave train. Such waves are termed wake fields. Free electrons are partially trapped by the plasma wake field and accompany it. Since the group velocity of the laser wave train, viz.

$$V = \frac{c}{\omega}\sqrt{\omega^2 - \omega_{\rm pl}^2}$$

(here, $\omega_{\rm pl}$ is the electron plasma frequency) is close to the speed of light c in a vacuum, the trapped electrons acquire a longitudinal ultrarelativistic energy.

The wake field produced has a short lifetime. In fact, the plasma wave can support a small number of trapped electrons without loosing its wave structure. Because of the high intensity (in the case of superstrong laser pulses), it is the nonlinear plasma wave which is destroyed when the wave crest stalls just after the first oscillation period, similarly to conventional high-amplitude hydrodynamic waves. This is also assisted by intense radial oscillations of electrons in the transverse electric field of the laser wave. The wave breakdown is a quick (nonadiabatic) event; hence, electrons keep their ultrarelativistic energies and continue their flight to the overdense plasma region.

Thus, the plasma wave is not periodical but has a first period only. The accelerated electrons may outrun not only the plasma wake field but also the laser pulse. The remaining positively charged cloud of atomic ions slightly slows down these electrons.

The length over which the electrons are accelerated has the form [36]

$$L = \frac{2c}{\omega_{\rm pl}}\left(\frac{\omega}{\omega_{\rm pl}}\right)^2,$$

and is well above the plasma wavelength, since $\omega \gg \omega_{\rm pl}$ in the underdense part of the plasma. The maximum energy of accelerated ultrarelativistic electrons is limited by the breakdown of the plasma wave [37]:

$$\varepsilon_{\max} = 4mc^2\left(\frac{\omega}{\omega_{\rm pl}}\right)^2. \qquad (25)$$

The maximum field intensity in the plasma wave is as follows [36]:

$$E_{\max} = \frac{m\omega_{\rm pl}c}{e}. \qquad (26)$$

An excitation of a plasma wave depends on the duration of the laser pulse. The excitation mechanism given above is realized when the laser pulse duration is shorter than the period $2\pi/\omega_{\rm pl}$ of the plasma wave. For long-duration laser pulses, the wake fields are excited in a rather different way: the electromagnetic wave of the laser pulse decays into a plasma wave and another electromagnetic wave in the process of stimulated Raman scattering.

Notice that most experiments devoted to wake-field investigation deal with gas targets in which all plasma has underdense density, rather than with solid targets.

Thorough measurements of electron spectra emerging in the interaction of laser pulses possessing an intensity from 10^{18} to 2×10^{19} W cm^{-2} with a gas jet (with the electron concentration ranging from 1.5×10^{18} to 1.5×10^{20} cm^{-3}) were performed in Ref. [38]. The laser radiation was linearly polarized and a laser pulse duration amounted to 35 fs. The maximum electron energy was as high as 70 MeV. This is in agreement with formula (25). The electron energy increases with the reduction in electron concentration, which also agrees with formula (25), and with an increase in the intensity of the laser pulse I (according to $E_{\max} \sim \sqrt{I}$). The latter fact is related to the direct mechanism of electron acceleration in the ultrarelativistic limit considered above.

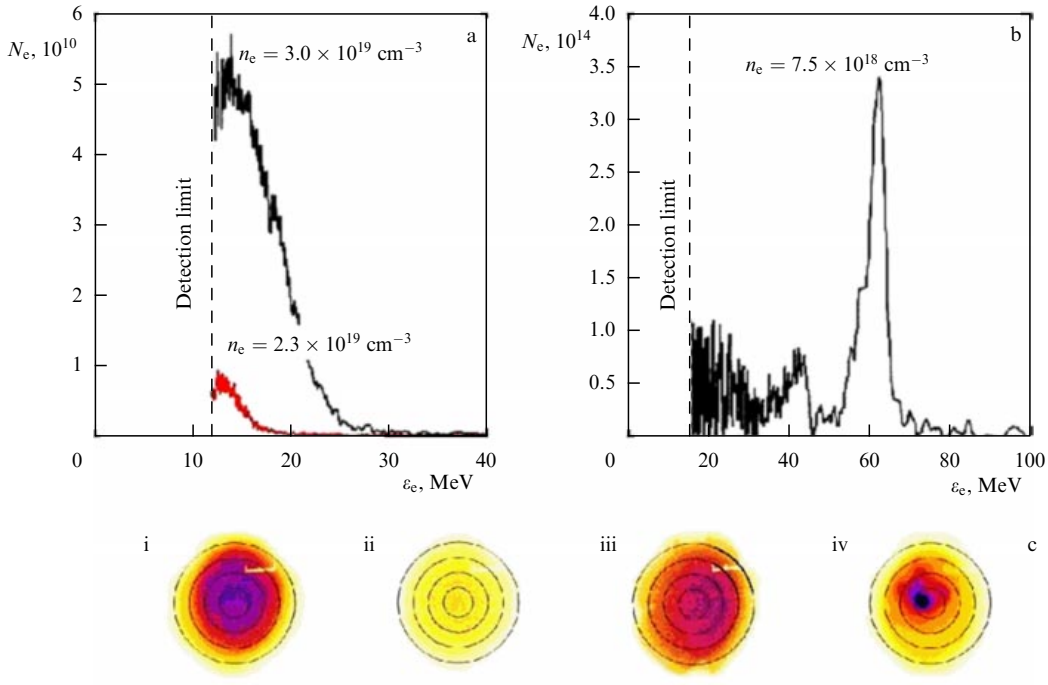

Figure 3. Electron spectra at (a) $n_e = 3.0 \times 10^{19}$ cm^{-3} and 2.3×10^{19} cm^{-3}, and (b) $n_e = 7.5 \times 10^{18}$ cm^{-3}; (c) the measured divergences of an electron beam at (i) $n_e = 3.0 \times 10^{19}$ cm^{-3}, (ii) $n_e = 1.5 \times 10^{19}$ cm^{-3}, (iii) $n_e = 3.0 \times 10^{19}$ cm^{-3}, and (iv) $n_e = 1.5 \times 10^{19}$ cm^{-3}. The interval between circles is ~ 10 mrad (N_e is the number of electrons per MeV per sr).

In work [39], the Ti:sapphire-laser pulses of the Astra setup (Great Britain) with an intensity of 5.5×10^{19} W cm^{-2} and a duration of 50 fs interacted with a gas beam of helium atoms. An intermediate regime was realized, in which the laser pulse duration was comparable to the period of the plasma wave. At the electron beam concentration of 7.5×10^{18} cm^{-3}, a sufficiently monoenergetic beam of ultrarelativistic electrons was observed with an electron energy of 60 MeV (see Fig. 3), which agrees with formula (25).

Nevertheless, on the other laser setup with a radiation intensity of 5×10^{18} W cm^{-2} and a pulse duration of 35 fs [40] at a higher electron concentration (2×10^{19} cm^{-3}), a sufficiently monochromatic beam of ultrarelativistic electrons with an energy of 150 MeV and a width of approximately 30 MeV was observed in a gas beam of helium atoms (helium atoms are completely ionized in a field of such intensity), as shown in Fig. 4.

In addition to the ponderomotive mechanism for generating plasma waves, the latter may be produced by the direct conversion of ultrashort optical laser pulses of relatively low intensity (10^{15} W cm^{-2}) into terahertz radiation with an intensity of up to 10^{19} W cm^{-2} [41].

The results of particle-in-cell simulations [42] provide support for the longitudinal ponderomotive acceleration of electrons, needed for producing a plasma wave, and also show that the electrons form a bunch following the laser pulse. Definitely, there is also a transverse ponderomotive acceleration of electrons, so that the bunch size is above the radius of the laser-beam focus spot [43]. In addition, electrons are trapped by the wake field provided that the electron concentration in the underdense plasma is above 10^{19} cm^{-3}. At lower concentrations, electrons are mainly pushed out by a ponderomotive force in the transverse direction relative to the laser beam.

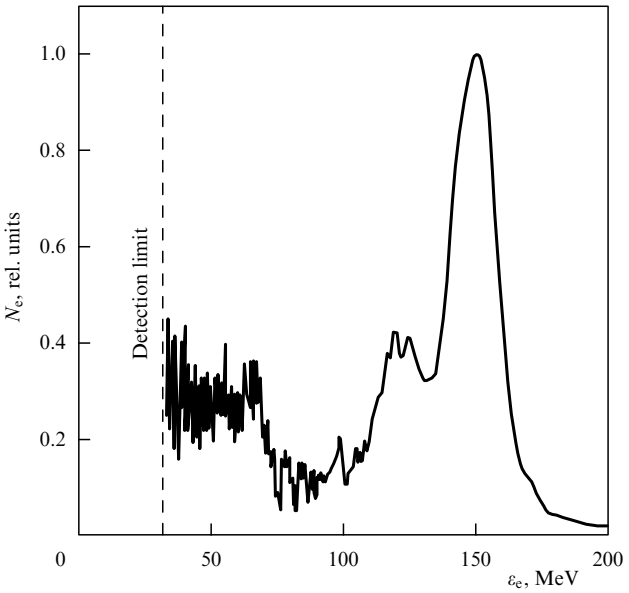

Figure 4. Example of the electron spectrum obtained at a plasma number density $n_e = 2.0 \times 10^{19}$ cm^{-3}, laser pulse duration $\tau = 35$ fs, and pulse energy $E = 600$ mJ (N_e is the number of electrons moving in the range of the relative energy $\Delta E/E$).

In a superstrong laser field, ultrarelativistic electrons also produce γ-quanta and positrons. Positrons are more strongly accelerated by the field of the plasma wave than electrons [44].

A plasma wake field may also shorten the laser pulse that produces this plasma wave. This phenomenon was observed in Ref. [45], where a laser pulse with a peak intensity of 3.2×10^{18} W cm^{-2} irradiated a gas beam of helium atoms and the pulse duration changed from 38 fs to 10 fs with an energy

efficiency of 20%. If the duration of the laser pulse is shorter than the period of the plasma wave, then the longitudinal ponderomotive force broadens the laser pulse spectrum and then compresses the pulse. At the leading edge of the laser pulse, the oscillation frequency shifts to the red spectrum range, and at the trailing edge of the pulse it shifts to the blue. Due to plasma dispersion, the trailing edge of the pulse moves faster than the leading edge, which provides the compression of the laser pulse.

The wake field is a source of X-rays. Electrons trapped by the wake field oscillate in a magnetic field produced by a moving electron bubble — this is none other than the betatron oscillations. According to the calculation performed in Ref. [46], such oscillating electrons produce radiation in a broad spectral range with maximum γ-quantum energy of about 50 keV at an intensity of the circularly polarized laser pulse of 10^{20} W cm^{-2} and a duration of 22 fs. The divergence of the γ-quantum beam is sufficiently small, being no more than about 0.1 rad.

In experiments [47], a high-intensity laser pulse (2.3×10^{19} W cm^{-2}) had a record short duration of 23 fs. A gas target with a plasma number density varying from 10^{19} to 1.4×10^{20} cm^{-3} was subjected to irradiation. It was found that the electron spectra are of a two-temperature character. One group of electrons had a temperature of 2.5 MeV, whereas the temperature of the other group reached 7.8 MeV. The authors explained this fact by different regimes of wake field breakdown. In one case, the wake field breaks in a homogeneous part of the plasma, and in the other case it breaks at the front of the shock wave produced by a laser prepulse.

Electron acceleration in a wake field produced by the action of a laser pulse on magnetized plasma was theoretically considered in paper [48], as was the problem of laser pulse stability with respect to plasma wave generation near the upper and lower hybrid plasma frequencies.

Concluding this section, we present Table 1 wherein the considered mechanisms of electron heating in dense media are given along with the conditions in which these mechanisms dominate.

Table 1. Comparison of various mechanisms for electron heating in dense media.

Heating mechanism	When dominant
Induced inverse bremsstrahlung in the scattering of electrons on ions	Intensities below 10^{15} W cm^{-2}
Longitudinal ponderomotive acceleration of electrons in a skin layer	Relativistic intensities above 10^{19} W cm^{-2}
Vacuum heating	High contrast, moderate intensities, short-duration pulses
Resonance absorption of laser radiation	Low contrast, long-duration pulses
Wake-field electron acceleration	Gas targets, large underdense plasma domain, ultrashort pulses
Cyclotron mechanism	Presence of an external constant magnetic field
Betatron mechanism	Vortex electric field produced by a varying magnetic flux that penetrates the electron orbits

3. Generation of fast protons and ions in the interaction of ultrashort high-intensity laser pulses with solid targets

In the previous section, we discussed various mechanisms of electron acceleration in the interaction of high-intensity laser pulses with solid targets. Electrons can move inward from the target surface or to the outside of it, i.e., towards the laser pulse. The Coulomb attraction of positively charged atomic ions to electrons results in a directed motion of the ions. This is the subject of our consideration in the present section.

First, consider how the flux of fast electrons produced by a superstrong laser pulse and directed into the depths of the target is decelerated in it. Electrons may either be completely (or partially) retarded in matter or freely pass across the whole target, depending on their kinetic energies. The main losses of fast electrons in the target are related to the collision ionization of target atoms. Under the assumption that the electron energy is on the order of 1 MeV and the energy transfer in each act of atomic ionization is below 10 – 20 eV, one can estimate the energy loss for a relativistic electron per unit path length using the Bethe – Bloch formula [49] (in atomic units):

$$\frac{\mathrm{d}\varepsilon}{\mathrm{d}z} = \frac{2\pi Z n_\mathrm{a}}{c^2} \ln \frac{c^2}{2\pi n_\mathrm{a}} . \qquad (27)$$

Here and in what follows, n_a is the concentration of target atoms, and c is the speed of light. At an electron energy reduced to nonrelativistic values, the ionization losses sharply increase, since in formula (27) the speed of light should be substituted by the lower velocity of a decelerating electron, $v < c$. For a fast electron with an energy of 1 MeV and the target atom concentration $n_\mathrm{a} = 10^{23}$ cm^{-3}, one sees from formula (27) that the track length is no longer than 1 mm. Hence, foils with a thickness of less than 1 mm can be considered definitely transparent for relativistic electrons.

In thicker targets, one should consider only those electrons which move from the target front surface in the underdense part of the plasma towards the laser pulse. They acquire transverse (with respect to the propagation direction of the laser pulse) ponderomotive energy related to the spatial distribution of the laser beam over the focus spot. In the case of inclined incidence of the laser pulse on the target, such electrons have the velocity component directed outwards from the target. But the motion of electrons is not narrow-directed: the electron concentration in the underdense part of the plasma is not high and it falls rather gradually to the outside of the target surface. These factors reduce the electron energy compared to the ponderomotive estimate. The energy of atomic ions entrained by the Coulomb attractive force of electrons reduces correspondingly. Thus, below we will concentrate on foils.

Ion acceleration in laser plasma produced by femto- and picosecond pulses is related to the emergence of strong quasistatic electric fields created by the motion of a fast electron bunch in the process of charge separation. Presently, three mechanisms are considered for accelerating atomic ions by electrons, when foils of a thickness 1 – 100 μm are hit with a laser pulse:

(1) acceleration of ions from the front foil surface towards the laser pulse (i.e., outwards from the target),

(2) acceleration of ions inward from the front surface of the foil target;

(3) acceleration of ions from the rear surface of the foil target outwards from it.

The first and second mechanisms are present in thicker targets as well, resulting, in particular, in the initiation of various thermonuclear reactions.

Ion acceleration by the first and third mechanisms occurs in the following way. In the case of the first mechanism, the beam of electrons directed outwards from the front surface of the foil entrains the atomic ions arising due to field ionization and residing in a skin layer. Lighter ions are mainly involved in the process, i.e., the protons produced at the foil surface from adsorbed oxides. The protons possessing an energy in the MeV range move from the front foil surface towards the laser pulse. In the case of the third mechanism, protons are produced at the back foil surface due to ionization by the quasistatic electric field of separated charges. The divergence of the beam of protons moving from the rear surface is narrower than that of the electron beam because the Coulomb repulsion between the protons has a weaker effect than between the electrons.

If the plasma boundary is sharp, then the characteristic distance in which the charges are separated is the Debye length. In the nonrelativistic case it is equal to

$$L_{\mathrm{D}} = \sqrt{\frac{\varepsilon_{\mathrm{e}}}{6\pi n_{\mathrm{e}} e^2}}. \tag{28}$$

This length is determined via the electron energy ε_{e}, because the concept of electron temperature may become inappropriate at high electron energies and short pulse durations. In the relativistic case, it is on the order of the skin layer thickness:

$$L_{\mathrm{D}} \sim \frac{c}{\omega_{\mathrm{pl}}}\,, \tag{29}$$

where ω_{p} is the relativistic plasma frequency (comprising the 'heavy' mass of an electron).

The outgoing electrons with the kinetic energy ε_{e}, flying away for a distance on the order of the Debye length, form a quasistatic electric field with the intensity

$$E_{\mathrm{D}} = \frac{\varepsilon_{\mathrm{e}}}{eL_{\mathrm{D}}}\,. \tag{30}$$

In relativistic laser pulses, this field is much stronger than the atomic electric field. Formula (30) is valid if the Debye length is longer than the characteristic dimension of plasma inhomogeneity at the front surface of the foil. In the opposite case, the Debye length in formula (30) should be replaced by the dimension of this inhomogeneity.

Thus, the mechanisms of ion (usually protons) acceleration are determined by the fields of the spatial charge induced by the motion of fast electrons. However, these fields substantially differ for the front and rear (back) foil surfaces. As noted above, the scale of these electric fields is determined, on the order of magnitude, by the ratio of the electron energy to the scale of plasma spatial inhomogeneity. At the front surface, this scale is mainly determined by the action of a pre-pulse and in typical experimental conditions the characteristic dimension of electron concentration inhomogeneity amounts to dozens of micrometers. Conversely, at the rear surface the scale of spatial charge separation is determined, according to formula (30), by the Debye length which runs into several micrometers in the same conditions. Evidently, this difference results in more efficient ion acceleration from the rear foil surface with the electric field intensity being on the order of 10 GV cm^{-1}, whereas at the front surface the ion acceleration and field intensity are several times lower.

Foils can be classified as thick or thin. In the first case, the foil thickness is greater than the extent of the laser pulse train: $c\tau \sim 30$ μm (for the laser pulse duration $\tau = 100$ fs). A portion of the electrons that escaped from the rear foil surface return to the target due to a self-induced electric field and then do not participate in the ion acceleration process.

Most promising is the second case in which electrons oscillate in a laser field while passing many a time through a thin foil back and forth [50]. In Ref. [50], the particle-in-cell simulation was utilized to study the generation of high-energy protons in the interaction of a short laser pulse with dense plasma having an interface with the underdense plasma produced by a pre-pulse. Proton acceleration in underdense plasma was calculated in the direction of the laser pulse propagation. The effect of the reverse electron motion towards the laser pulse at the rear foil surface was also exposed.

It has been shown [50] that the maximum proton energy increases with reducing foil thickness due to a greater concentration of hot electrons at the rear side of the target. A skin layer is actually absent, not disturbing the propagation of a train of laser pulses, because a superstrong relativistic laser pulse noticeably increases the depth of a skin layer, pushing electrons out from the laser pulse axis to the periphery by the action of a transverse ponderomotive force. The maximum conversion of the laser energy into the electron energy occurs at the laser pulse duration of 10–30 fs. In multiple passages through the thin foil back and forth, electrons acquire no additional energy from the laser field. On the contrary, they lose it due to collisions.

In the second mechanism of ion acceleration inward from the front foil surface, the accelerating field strength is determined by the electron energy acquired due to the ponderomotive acceleration in a underdense part of the plasma or due to vacuum heating in the case of a sharp foil–vacuum boundary (for a laser pulse impinging obliquely on the foil surface; see the previous section). In the nonrelativistic case, this energy for linearly polarized light field is given by

$$\varepsilon_{\mathrm{e}} = \frac{e^2E^2}{2m\omega^2}\,. \tag{31}$$

Dividing this energy by the wavelength c/ω of laser radiation (the characteristic inhomogeneity dimension in the case of a sharp foil–vacuum boundary) we obtain the intensity of the quasistatic accelerating field:

$$E_{\mathrm{s}} = \frac{e^2E^2}{2cm\omega}\,. \tag{32}$$

In the relativistic case, the mass of an electron m in this formula should be substituted by the 'heavy' mass:

$$m \to m\sqrt{1+\frac{1}{2}\left(\frac{eE}{mc\omega}\right)^2}\,. \tag{33}$$

Estimates made for ultrarelativistic laser fields show that the quasistatic field intensity is of the same order of magnitude as for the laser field.

Protons following electrons acquire the same kinetic energy as electrons (whereas atomic ions with the charge Z acquire Z times greater energy), much as in the case of ion sound in a plasma. Such a situation, of course, is only possible

if the time needed for protons to acquire the kinetic energy is shorter than the duration of the laser pulse. This time in atomic units is given by [50]

$$\tau_s = \frac{2\pi}{\omega_{pl}} \sqrt{\frac{M\omega c}{eE}}. \tag{34}$$

Here, M is the proton mass, and E is, as stated above, the electric field strength for the laser wave. At the radiation intensity 10^{19} W cm^{-2} of a Ti:sapphire laser, time τ_s is equal to 90 fs. If protons acquire kinetic energy in a time longer than the laser pulse duration, then the kinetic energy of the protons should be reduced by a factor of τ_s/τ, where τ is the duration of the laser pulse. These considerations are valid for both the second and third mechanisms of ion acceleration.

The electrostatic field considered accelerates protons toward the interior of the target. In addition, in dense foil the laser pulse 'perforates' the material, producing 'dents'. The resulting depth of laser pulse penetration into the foil noticeably increases compared to the standard depth of a skin layer. The maximum ion energy in this case is obtained from the simplest estimates for the momentum acquired by an ion under the action of a ponderomotive force in the overdense (in density) region [51]:

$$E_i^{max} \approx 2\sqrt{2} aZmc^2, \tag{35}$$

where a is the dimensionless parameter of the field intensity.

One can estimate this maximum energy acquired by protons at the front side of the foil (or in thick targets). By assuming that most of the laser energy reflects from a dense plasma, we obtain the simple expression $2I/c$ for the laser pulse pressure to the target. This pressure is equal to the proton momentum flux density $M_p v_p v_p n_p$, where M_p is the mass of a proton, v_p is its velocity, and n_p is the concentration of protons, which is equal to that of the electrons, n_e. Indeed, the momentum of an electron is negligible compared to that of a proton. The relationship mentioned, of course, expresses only the momentum flux conservation law and implies no direct energy transfer from laser to protons. As noted above, the laser energy is transferred to the protons (or to the atomic ions) through the electrons. Thus, for the proton kinetic energy E_p we have the following expression

$$E_p = \frac{I}{n_e c}.$$

The momentum is transferred on the critical surface of the laser plasma, where $n_e = m\gamma\omega^2/4\pi e^2$. In the relativistic case, we substituted here the mass of an electron by 'heavy' mass: $m \to m\gamma$, with $\gamma = \sqrt{1 + a^2/2}$. Introducing, as was done above, the dimensionless amplitude $a = eE/m\omega c$ of vector potential, we find $E_p = mc^2 a^2/2\gamma$. In particular, in the ultrarelativistic limit we obtain $E_p = mc^2 a/\sqrt{2}$.

However, this proton energy is not maximal. At the superstrong intensity of a laser field, the proton velocity v_p exceeds that of ion sound. Hence, the plasma critical surface propagates along the laser pulse direction at the velocity v_p, composing a shock wave. Protons that have passed through this wave may change the direction of their velocity v_p to the opposite one under the action of the Coulomb forces from the side of electrons tending to keep an electrical neutrality of the plasma. The protons falling back to the critical surface and elastically reflecting from it in the direction of laser pulse propagation acquire the velocity $2v_p$. Consequently, the maximum energy of a proton is 4 times the value given above. Finally, in the ultrarelativistic limit we obtain the energy of protons moving in the direction of laser pulse propagation in the form

$$E_p = 2\sqrt{2} mc^2 a.$$

As follows from the three mechanisms considered above, the highest ion acceleration is achieved at the rear foil surface.

These conclusions are confirmed by thorough experimental investigations of proton acceleration mechanisms [52] performed using the petawatt laser setup at Livermore National Laboratory (USA) with pulse durations ranging from 0.5 to 5.0 ps and a relativistic intensity of up to 3×10^{20} W cm^{-2}. Both thick solid targets of 1 mm in thickness, made from Au, and thin solid targets from Au and CH of 50–125 μm in thickness were irradiated. Energy spectra and angular distributions were measured for electrons and photons. About 40–50% of the laser energy was converted into a beam of hot electrons with wide divergence. Approximately 3×10^{13} protons were observed with an energy of several dozen megaelectron-volts, their total energy being $\sim 6\%$ of the laser pulse energy for foils made from Au and CH with thicknesses ranging from 50 to 125 μm. The maximum proton energy was 55 MeV. Protons escaped from the rear surface of the foil. The divergence angle of a proton beam was rather small and reduced with the proton energy. Proton emission from the front foil surface was noticeably weaker and did not exhibit narrow divergence. Hot electrons formed the Debye layer in which the electrostatic field strength was several megavolts per micrometer. This field efficiently accelerated protons.

Two experimentally registered facts confirm the above conclusions concerning the efficiency of proton acceleration from just the rear surface of a foil, namely, (1) accelerated protons are always emitted normally to the rear surface of a foil regardless of the geometry of laser beam incidence, and (2) protons are detected even with gold foils in which they can only arise from molecular compounds adsorbed on the rear surface of a target, because the front surface is completely cleaned from these compounds by a thick layer of a preplasma. The experimental energy spectra obtained for accelerated protons sufficiently well correlate on the whole with the described mechanism of their acceleration.

The authors of work [53] observed protons with a maximum energy of 30 MeV in the interaction of laser pulses of an intensity $\leqslant 5 \times 10^{19}$ W cm^{-2} with the plasma of a solid target, which was produced on the surface of a thin aluminium foil 125 μm in thickness. At the rear surface of the target, about 10^{12} protons were detected with an energy above 2 MeV. Angular divergence was measured for the proton beam. Similar measurements were performed for protons emitted from the front surface of the foil. Based on the results of measurements with activation and track detectors, the authors of work [53] made a conclusion that the protons escaping from the rear surface of the foil are produced at its front surface. They are deflected by strong magnetic fields inside the plasma. These fields are induced by the flux of fast electrons which are generated by the laser pulse. The experiments described in Ref. [53] allow one to conclude that the thermonuclear reactions observed are caused by the plasma flux effects. From ion energy measurements it also follows that the Weibel instability is absent in the experiment. Nevertheless, the diffusion of magnetic fields

inside a target smooths large inhomogeneities in a shorter time than it takes for protons to travel through the magnetized region. Such instabilities in electron jets can only exist in a small region near the front foil surface.

From experiments [53] it follows that there are two different components of high-energy protons and other ions accelerated on the front foil surface inside a plasma bunch. Protons with lower energies are produced in the course of many picoseconds after termination of a laser pulse, when the plasma bunch is released; they are strongly influenced by the magnetic fields generated in the plasma bunch.

The high-energy part of protons observed from both the front and rear foil surfaces is initially accelerated during the laser pulse. The initial acceleration of both protons and heavy ions is caused by high-power electrostatic fields generated due to the longitudinal ponderomotive charge separation in a skin layer and to intensive generation of longitudinal plasma waves in a pre-plasma. Their subsequent acceleration is caused by electrostatic fields generated by fast electrons escaping from the interaction region.

The authors of paper [54] irradiated thin Al foil 1.8 μm in thickness with a subpicosecond laser pulse with high contrast $K \cong 10^7$ at the maximum laser radiation intensity of 3×10^{18} W cm^{-2}. Electron acceleration inside the foil follows the vacuum heating mechanism (see the previous section). Due to charge separation, an accelerating electric field arises with an intensity on the order of 10^{10} V cm^{-1}. The authors of Ref. [54] reached the conclusion that the protons arising from impurities at the front surface of a foil are accelerated inside it and escape from the rear side of the foil normally to its surface. A beam of protons with an energy of about 1.5 MeV propagates within a cone with a vertex angle of $40 \pm 10^\circ$. The maximum energy of protons is explained by their acceleration in the electrostatic field caused by spatial charge separation due to vacuum heating. It is assumed that when the high-intensity laser pulse is incident on the surface of the target, it produces a pre-plasma wherein longitudinal electron oscillations arise, caused by an oscillating magnetic part of the Lorentz force $\mathbf{v} \times \mathbf{B}$. Near the target surface these electrons escape from the target and come back into it. This occurs twice during the period of laser field oscillations. The Lorentz force rapidly decays inside the target. The returning electrons are accelerated in a underdense part of the plasma by the electric field of a laser wave and, moving at relativistic velocities, transfer their energy toward the target interior. Thus, a jet of high-energy electrons is formed with a low concentration.

In irradiating solid Pb targets 2 mm in thickness and Al targets 125 μm in thickness with a focused laser pulse with an intensity of 5×10^{19} W cm^{-2}, the authors of Ref. [55] observed heavy lead ions with an energy of up to 430 ± 40 MeV. In the energy spectrum of ions (see Fig. 5), a high-energy component was detected, which was caused by ion acceleration in the electrostatic field of separated charges. In addition, a low-energy component was observed, which formed a ring created by magnetic fields in a heated plasma released.

In Fig. 6, a spectrum of ions is presented in which both peaks and plateaus are seen at energies above 4 MeV [55].

In the experimental work [56], laser pulses irradiated CH foil with a thickness of 100 μm at the peak laser pulse intensity of 3×10^{20} W cm^{-2}. It was found that 12% of the laser energy is transferred to 2×10^{13} protons possessing an energy above 10 MeV. On the axis of the proton beam, the energy spectrum

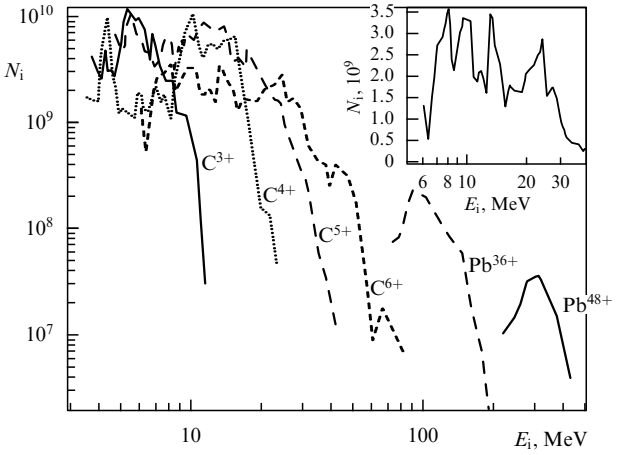

Figure 5. Experimental spectra of carbon and lead ions [55]. The spectrum of the C^{6+} ion is plotted on a linear scale in the inset. (N_i is the number of ions per MeV per sr.)

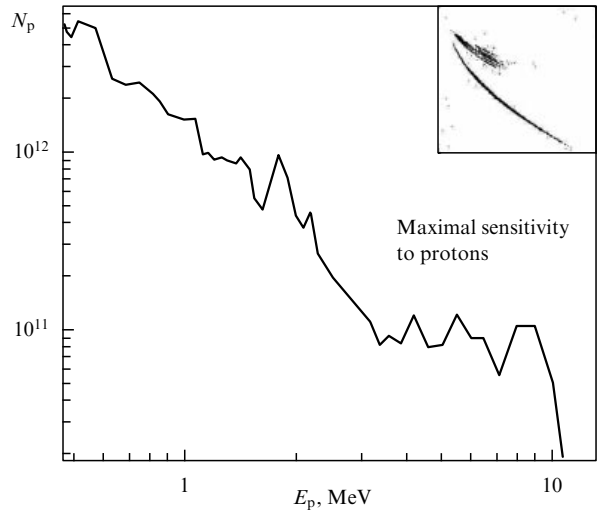

Figure 6. Proton spectrum indicating multiple peaks and plateaus at energies above 4 MeV. Data obtained with the use of the Thomson parabola are given in the inset. (N_p is the number of protons per MeV per sr.)

of the protons has a cut-off at a proton energy of 58 MeV. The proton energy decreases away from the beam axis.

At the top of Fig. 7 is presented a proton spectrum taken at a normal incidence of laser pulses on a CH target [56]. At the bottom, the spectrum of protons is shown recorded by a magnetic spectrometer along the axis and at the angle of 45° to it. Thermonuclear reactions initiated by the protons were detected. The authors of Ref. [56] reached the conclusion that the light pressure at the front surface of the target in the laser focus spot cannot generate the ions detected since there is the definite certainty that the protons are emitted from the rear surface of the target. The flux of protons from gold plate targets was greater than that from adsorbed layers in the focal plane. Anyway, a pre-pulse would clean the surface.

In theoretical article [51], 3D particle-in-cell simulations were made for studying ion acceleration in a foil irradiated with a laser pulse with an intensity of 10^{19} W cm^{-2}. At the front foil surface, a longitudinal ponderomotive force draws electrons in toward the foil interior, thus inducing an electric field due to charge separation. This field accelerates atomic

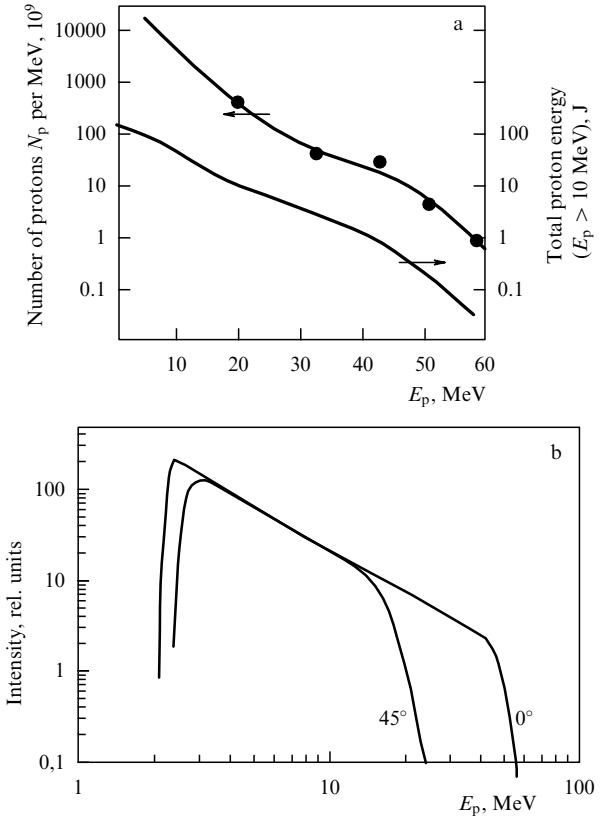

Figure 7. (a) Proton energy spectrum obtained at normal incidence of a laser pulse with an energy of 432 J on a 100-μm thick CH target. (b) Proton energy spectrum recorded with a magnetic spectrometer. The two plots show the spectra taken along the axis and at an angle of 45° to it.

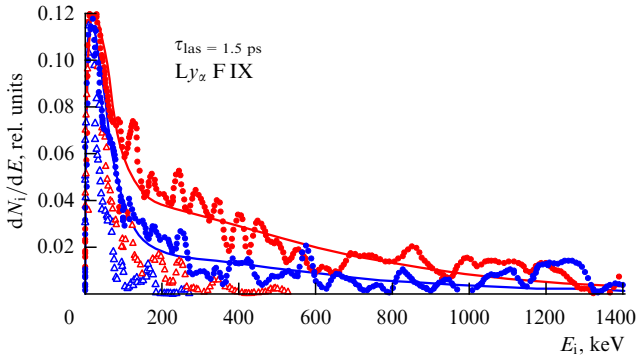

Figure 8. Energy distribution of fast fluoride ions derived from the profile measurements of Ly_α line emitted by F IX ion. Top curve corresponds to ions moving towards the target, while bottom curve refers to ions moving outward from the target.

ions. At the rear surface of the foil, ions are accelerated by the spatial charge of hot electrons emitted into a vacuum [52]. It was found that the magnetic fields generated by an electron jet in the overdense plasma noticeably influence the movement of the electron jet itself. Fast ions escape from the rear foil surface within a narrow cone, which agrees with the experiments [55] discussed above.

The calculated results of Ref. [57] confirm the mechanism in which hot electrons produced at the front foil surface pass through the foil and ionize a hydrogen layer at the rear foil surface. The powerful pre-pulse of a petawatt laser creates a large plasma domain in front of the foil surface. A bunch of electrons with energies ranging from 1 to 10 MeV is produced as soon as the main pulse reaches the target. The electron bunch draws protons with itself from both the front and rear foil surfaces. The protons from the rear surface are more strongly accelerated due to a higher plasma density gradient and, in addition, the beam divergence for these protons is narrower than that for protons from the front surface. Certainly, the target should not be too thin in order to prevent the pre-pulse from reaching its rear surface. Nevertheless, the target should not be too thick either, because electrons would be decelerated inside it. Hot electrons should be produced in, at most, 1 ps for preventing an enlargement of the plasma layer at the rear foil surface due to substance heating. Protons are accelerated, according to Ref. [57], in less than 10 ps at a distance on the order of 10 μm from the rear foil surface. Thus, the protons produced are accelerated by the bunch of hot electrons emitted from the foil to energies of ten or more megaelectron-volts at a distance on the order of ten micrometers.

In work [58], the authors measured the energy and angular distributions of protons emitted from the rear surface of a plastic foil subjected to irradiation with an intense laser pulse. For targets with a thickness of 5 μm, the number of protons observed with an energy of 3 MeV amounted to 1.8×10^9. In this case, a strong toroidal magnetic field arose behind the rear target surface, which deflected the protons and resulted in an annular structure of proton emission.

In Ref. [59], the dependence of proton energy on the intensity of laser radiation in irradiating a thin plastic foil by superstrong femtosecond laser pulses was discussed. It was experimentally shown that protons with higher energies are emitted in the direction of laser pulse propagation rather than in the opposite direction. The maximum proton energy depended on the intensity I of the laser pulse as $I^{0.5}$ up to 2 MeV at $I = 10^{18}$ W cm^{-2}.

In paper [7], experimental data are presented on the generation of fast ions in a laser picosecond plasma at a laser radiation intensity of 2×10^{18} W cm^{-2}. The results were obtained from Doppler spectra of hydrogen-like fluoride ions. An important peculiarity of the energy distribution of fast fluoride ions is the slow fall in ion energy to 1.4 MeV. In Fig. 8, the energy distribution of fast fluoride ions is plotted based on the results of measurements of Ly_α line profile for F IX ion. The solid curves are calculated by the formula

$$\frac{dN}{dE} \sim \exp\left[-\frac{M(v-v_0)^2}{2T_{fast}}\right], \qquad (36)$$

where v is the ion velocity in the observation direction, $Mv_0^2/2 = 25$ keV, and the temperature of the fast fluoride ions is $T_{fast} = 350$ keV.

In addition, using the red shift of the Doppler profile for the Ly_α line it was found that fast ions move inwards from a target surface. In Ref. [7], the parameters of the fluoride ion energy distribution were also estimated theoretically.

Notice that the directed motion of fast ions toward the interior of the target may result in the initiation of various nuclear reactions inside it. For example, the generation mechanism for neutrons in the process of deceleration of a fast deuteron in the medium comprising deuterium was thoroughly analyzed in Ref. [60].

In work [61], the results of experiments performed at the 100-terawatt laser setup at LULI Laboratory (France) are

presented. By varying the geometry of the rear surface of a target, the authors succeeded in significantly changing the shape and quality of a proton beam for radiography applications.

The influence of the plasma density gradient on the production of MeV-range protons in thin foils irradiated with a laser with an intensity of 5×10^{19} W cm^{-2} is discussed in Ref. [62]. If plasma is absent, then protons with an energy above 20 MeV form a tail in the exponential energy spectrum with a temperature of 2.5 MeV. When a plasma layer 100 μm in thickness is produced on the rear foil surface, the maximum energy of the protons reduces to 5 MeV and the proton beam noticeably scatters. The experimental results agree with the conception of the electrostatic mechanism, which requires an ultrathin plasma domain at the rear surface of a target. The maximum proton energy and ion acceleration efficiency strongly depend on the existence of a large gradient of plasma density at the rear surface of the target. The experimental data completely agree with the mechanism of electrostatic acceleration and with particle-in-cell simulations. This is an important conclusion because it directly demonstrates the fact that manipulations with the rear surface of a thin target may substantially change the energy and spatial distribution of protons. Such manipulations may be used for concentrating a proton beam in a prescribed narrow energy range for various applications.

In the next article issued by the same group [63], the authors experimentally studied the relationship between proton energy and target thickness. Foils were irradiated by a laser with a pulse duration of 100 fs, peak intensity of above 1×10^{20} W cm^{-2}, and high contrast of 10^{10}. At a foil thickness of 100 μm, the energy spectrum of protons was characterized by a temperature of 1.4 MeV and maximum energy of 6.5 MeV. As the target thickness was reduced to 3 μm, the proton temperature increased to 3.2 ± 0.3 MeV, and the maximum proton energy amounted to 24 MeV. This result also agrees with the mechanism discussed above on the stronger generation of MeV-range protons in ultrathin foils.

Figure 9 depicts the maximum proton energy versus target thickness, obtained from experiments [63] and from 2D particle-in-cell simulations.

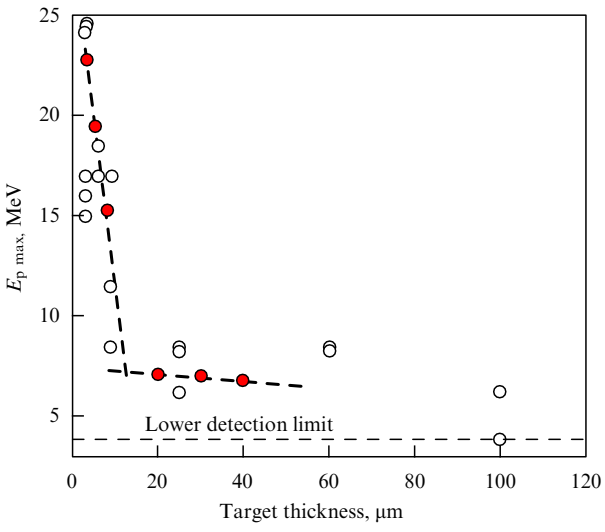

Figure 9. Peak proton energy versus target thickness obtained in experiments (○) and 2D particle-in-cell simulations (●).

In Ref. [64], low- and high-energy portions of proton spectra were studied experimentally for the case of interaction of superstrong laser pulses with thin foils. One part of the high-energy protons has a specific annular structure and is associated with the proton source residing at the front surface of the foil. Another part of the proton beam arises at the rear foil surface and exhibits very narrow divergence. Low-energy protons with a large angle of divergence were also observed.

The process of ion acceleration at the rear foil surface is surprisingly well described by the model of plasma expansion into a vacuum [66–67]. This process can be qualitatively described by a 1D model of plasma expansion into a vacuum. The model is based on the conception that the electron density obeys the standard Boltzmann distribution with some effective temperature T_e. The motion of ions is described by standard 1D hydrodynamic continuity equations and equations of motion for the ion velocity v_i and concentration n_i (p is the pressure):

$$\frac{\partial n_i}{\partial t} + \frac{\partial n_i v_i}{\partial z} = 0\,,$$
$$n_i\left(\frac{\partial v_i}{\partial t} + v_i\,\frac{\partial v_i}{\partial z}\right) = -\frac{\partial p}{\partial z} = -c_s^2\,\frac{\partial n_i}{\partial z}\,, \qquad (37)$$
$$c_s = \sqrt{\frac{ZT_e}{M_i}}\,.$$

The parameter c_s is the velocity of ion sound, Z is the ion charge, and M_i is the ion mass. The solution to these equations results in the simple law for the temporal dependence of ion velocity: $v_i = c_s + z/t$. It is responsible for the motion of a plasma front at the velocity of sound. The solution for the ion concentration is also written in the simple form

$$n_i = n_{i0}\exp\left(-\frac{v_i}{c_s}\right),$$

where the parameter n_{i0} corresponds to $v_i = 0$, i.e., to the unperturbed electron Debye radius $L_{D0} = \sqrt{T_e/4\pi Z n_i}$. From this expression for the ion concentration, one can obtain the current local Debye radius:

$$L_D = L_{D0}\exp\left(\frac{v_i}{2c_s}\right).$$

In addition, we have $L_D = c_s t$. Thus, we find

$$v_i = 2c_s\ln(\omega_{pli}t)\,.$$

Here, ω_{pli} is the ion plasma frequency. It is equal to

$$\frac{c_s}{L_{D0}} = \sqrt{\frac{T_e}{4\pi M_i n_i}}\,.$$

By using the maximum ion energy during the laser pulse $t = \tau$, we find the characteristic energy acquired by ions [65, 67, 68]:

$$E_i^{max} = 2ZT_e\ln^2(\omega_{pli}\tau)\,. \qquad (38)$$

The accelerating electric field E at the front of the ion pulse expanding into a vacuum has the characteristic scale

$$E = \frac{T_e}{ec_s t} = \frac{T_e}{eL_D}\,, \qquad (39)$$

i.e., is determined by the local inhomogeneity dimension of the expanding plasma.

In typical conditions of experiments with high-power femtosecond laser pulses, the number of accelerated protons per laser pulse is on the order of 10^{13}.

The ion acceleration model under discussion, with certain modifications, as noted above is in very good agreement with experiments [67, 69, 70].

In irradiating thin foils with a laser light [69], the influence of the laser pre-pulse caused by amplified spontaneous emission on proton acceleration was studied. The authors showed how one can choose the pre-pulse duration and optimal foil thickness for obtaining the maximum energy of a proton beam. In ultrathin foils, a pre-pulse forms plasma at the rear foil surface; in this case, protons are accelerated at the front foil surface to relatively low energies.

In paper [71], the degree of proton beam laminarity was measured on the irradiation of thin metal foils with a superstrong laser pulse. It was found that the degree of laminarity was approximately 10^4 times better than that obtained with ordinary ion beams from accelerators. The beam laminarity was only disturbed by weak collisions with fast electrons. At a proton energy above 10 MeV, the measured lateral dimension of the proton beam at the rear foil surface was below 10 μm. The authors in Ref. [71] emphasize that the reduction in proton beam divergence at a greater proton energy is related to the narrowing of the proton emitting zone at the rear target surface, rather than to a deflection in a magnetic field [53, 58, 64]. The authors of paper [71] also note that the interpretation [53, 58, 64] of the origin of annular structures due to magnetic fields is not correct.

In Ref. [72], experimental results are presented concerning the dependence of proton acceleration on the duration and intensity of a laser pulse in irradiating a copper foil with a thickness of 5 μm. The laser pulse intensity varied from 8.5×10^{17} to 1.1×10^{19} W cm^{-2}, and the duration was from 55 to 400 fs. It was found that the maximum proton energy increased at a longer pulse duration and fixed intensity of laser radiation, as it did at an increased intensity and fixed pulse duration.

In Fig. 10, the energy spectra of protons [72] are displayed for various pulse durations at a fixed pulse energy and a fixed intensity of the laser pulse. Dependence of the maximum proton energy is also shown versus the laser pulse duration τ_{las}.

Proton acceleration was studied in theoretical work [73] by particle-in-cell simulations in the interaction of superstrong laser pulses with foils of various thicknesses. At a laser radiation intensity on the order of 10^{20} W cm^{-2}, the maximum energies are acquired by protons due to the relativistic transparency of a heated thin foil.

In fundamental work [68], the measurement results are presented for the energy spectra of protons emitted from the front and rear surfaces of a metal foil when exposed to a laser pulse with an intensity of $\sim (1-6) \times 10^{19}$ W cm^{-2}. The conclusions made earlier that the protons accelerated from the rear foil surface form higher-energy and more dense jets with lower divergence than those accelerated from the front surface were confirmed. In this work, for the first time the mechanisms of ion acceleration from the front and rear surfaces of a thin foil were directly and quantitatively compared in similar conditions of laser action. The conclusion made in Ref. [53] and Ref. [64] that the protons with

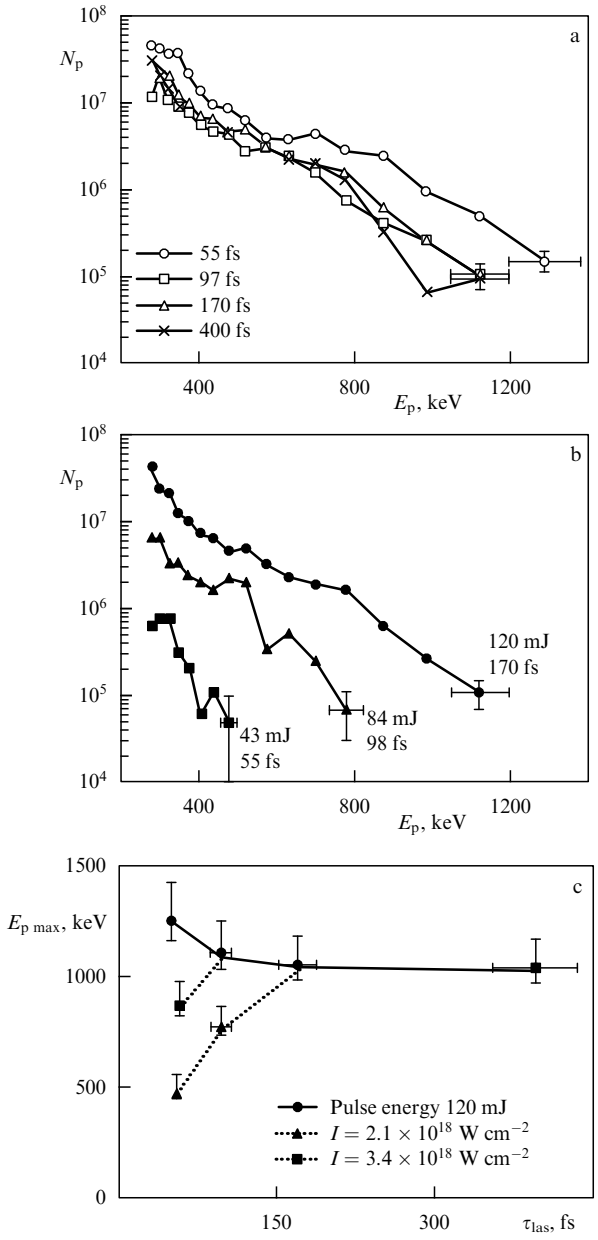

Figure 10. Proton energy distributions: (a) for different laser pulse durations at a constant pulse energy of 120 mJ, (b) at a constant laser pulse intensity of 2.1×10^{18} W cm^{-2}; (c) maximum proton energy $E_{p,max}$ versus the laser pulse duration τ_{las}. Circles correspond to the case of constant energy, while triangles and squares correspond to a constant intensity of laser pulses.

maximum energies are produced at the front foil surface is considered by the authors of Ref. [68] as wrong.

The authors of Ref. [68] in their later work [67] optimized the thickness of irradiated aluminium foil (target) and the intensity (energy) and duration of laser pulses for obtaining the maximum energy of accelerated protons.

In Fig. 11, the maximum proton energy is plotted versus the thickness of a target made from aluminium foil and exposed to a laser pulse 320 fs in duration with an intensity of 4×10^{19} W cm^{-2} [67].

One can see that there exists an optimal foil thickness which corresponds to the maximum efficiency of ion acceleration. At a smaller thickness, the shock wave produced by a laser pre-pulse substantially destroys the structure of the rear

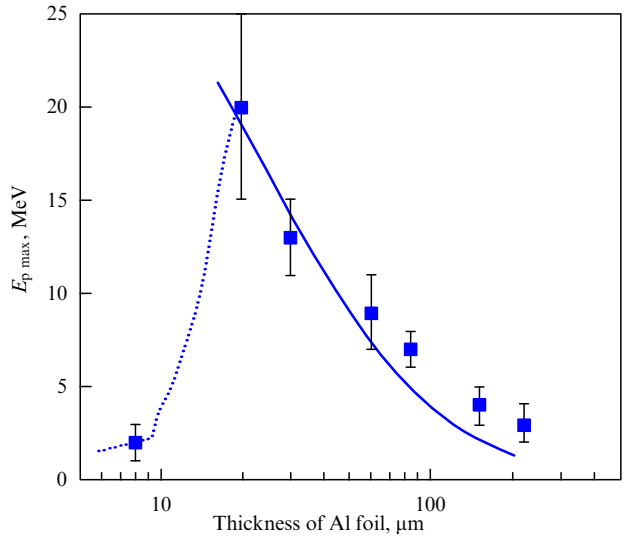

Figure 11. Maximum energy of protons accelerated with a laser pulse with an intensity of 4×10^{19} W cm^{-2} and duration of 320 fs versus the thickness of aluminium foil. Solid curve corresponds to a hydrodynamic simulation; dotted curve corresponds to the trace of experimental data denoted by the squares.

target surface, thus preventing the origin of a uniform accelerating layer of spatial charge. At a greater thickness, the origin of such a layer is also hindered due to electron deceleration inside the target material.

The energy of accelerated protons noticeably increases at longer laser pulse durations (at a constant intensity of the pulse). This tendency is demonstrated in Fig. 12 for three different intensities of laser pulses. The energy of laser pulses was increased with pulse duration in order to provide constant intensity in each experiment. As a whole, the results presented confirm the possibility of optimizing the energy of accelerated ions, although such optimization is connected with the duration and contrast of the pulses.

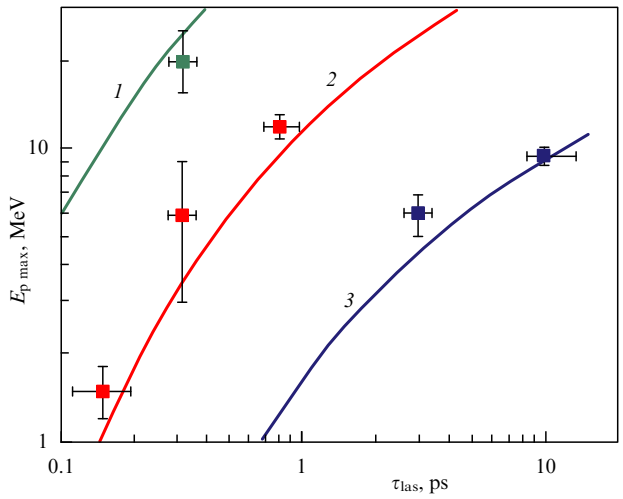

Figure 12. Maximum energy of accelerated protons versus laser pulse duration at three different intensities of laser radiation: (*1*) 6×10^{19} W cm^{-2}, (*2*) 1×10^{19} W cm^{-2}, and (*3*) 2×10^{18} W cm^{-2}. Solid curves correspond to a hydrodynamic simulation.

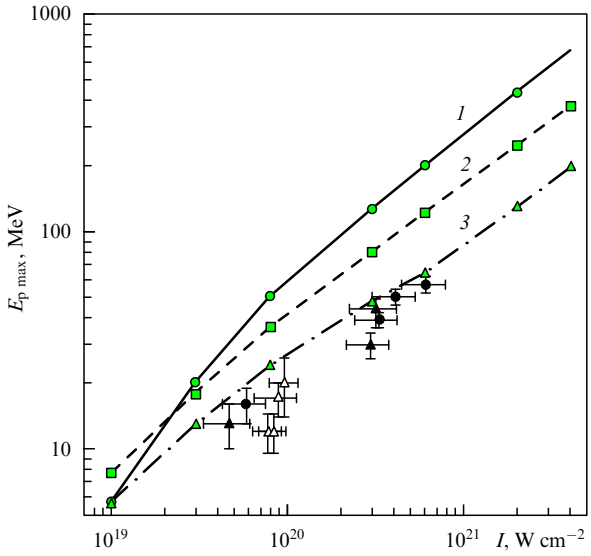

Figure 13. Maximum proton energy versus laser radiation intensity obtained by using: (*1*) the isothermic model, (*2*) the two-phase model, and (*3*) the two-phase model with 3D effects. Experimental points • and ▲ correspond to Al targets with thicknesses of 10 and 25 μm, respectively, at a pulse duration of 1 ps; the data points designated by △ correspond to an Al target with a thickness of 25 μm at varied pulse durations.

The authors of recent work [70] expanded the energy and intensity ranges of lasers up to 400 J and 6×10^{20} W cm^{-2}, respectively, for observing proton spectra. It was found that the proton energy increases more slowly than was predicted earlier (see Fig. 13). The two main parameters, namely, the maximum proton energy and the efficiency of converting the laser energy to proton energy were studied as functions of various parameters of laser radiation. The maximum proton energy was measured as a function of the laser radiation intensity in the range from 4×10^{19} to 6×10^{20} W cm^{-2} for aluminium targets with thicknesses ranging from 10 to 25 μm. The pulse duration was maintained constant at 1 ps, whereas the laser energy and, consequently, intensity varied. The maximum proton energy E_p changed from 10 to 55 MeV. The simple power expansion was found for approximating this energy as a function of intensity I: $E_p \sim I^b$, where $b = 0.5 \pm 0.1$. Thus, the maximum proton energy is proportional to the temperature of fast electrons, which varies as the ultrarelativistic ponderomotive potential $(I\lambda^2)^{1/2}$. Similarly to most previous experiments, a pre-plasma was produced at the front surface of the target due to the fact that a low-intensity laser pre-pulse reached the target prior to the main pulse doing so.

In Ref. [74], 2D and 3D particle-in-cell simulations were performed for the generation of fast ions under the action of high-power ultrashort laser pulses impinging on laminated targets of various densities and thicknesses. The simulations were aimed at finding an optimal target for obtaining ions with the maximum energy at a prescribed energy of the laser pulse. The calculations were performed for currently record laser pulse intensities.

Experiments on the irradiation of spherical atomic clusters with diameters below 1 μm by superstrong femtosecond laser pulses [60] are close to the subject of the present section. Ions with energies in the MeV range are produced as a result of the Coulomb explosion of such clusters.

4. Measurements of superstrong quasistatic magnetic fields in laser plasma and their theoretical interpretation

Mechanisms of generating magnetic fields are a subject of numerous investigations performed in recent years [1, 2, 75]. Various mechanisms for generating a magnetic field in the interaction of intensive laser radiation with solid targets are described in a number of theoretical works [76 – 83]. In particular, they predicted the origin of magnetic fields with induction of up to 1 GG in the dense plasma produced during the interaction process. These fields are localized near the critical surface, where the laser energy is mainly absorbed. The arising magnetic fields noticeably affect the dynamics of laser plasma. The principal mechanisms of generating quasistatic magnetic fields were considered: (1) different directions of the temperature and plasma density gradients; (2) the flux of fast electrons accelerated by ponderomotive forces in the longitudinal and transversal directions with respect to the direction of laser pulse propagation, and (3) the collisionless Weibel instability [84].

The generation of magnetic fields with induction of up to 1 GG in relativistic dense plasma was first predicted in Ref. [80]. According to the theory elaborated in this work, the source of a quasistationary magnetic field is the ponderomotive force acting on electrons. It gives rise to the radial electron current directed from the axis of a laser beam to the periphery, until the mutual oscillating movement of ions and electrons starts due to the electrical neutrality requirement.

One possible mechanism for generating spontaneous magnetic fields comprises the development of Weibel type instabilities [84]. A consistent kinetic study of the Weibel instability in plasma created by a superstrong femtosecond laser pulse was performed on the basis of solutions to the Maxwell – Vlasov equations [83, 85]. Both linear and circular polarizations of laser radiation were considered, with allowance made for relativistic effects. Collisions of nonequilibrium electrons with ions and thermal electrons were also taken into account. The maximum intensities of quasistationary magnetic fields of the Weibel type were estimated, as well as their characteristic scales.

The Weibel instability increment in the case of circular polarization of laser radiation is much greater compared to the case of linear polarization. For example, for laser radiation with the intensity of $\sim 10^{19}$ W cm^{-2} and intrinsic induction of 285 MG, the induction of the magnetic field arising in plasma in the case of circularly polarized radiation amounts to $B = 230$ MG (the spatial scale is 85 Å), whereas in the case of linearly polarized radiation it equals $B = 70$ G (the spatial scale is 240 Å). The Weibel magnetic field (in which the quasistatic electric field is weak compared to the magnetic field) is generated in plasma with a polarization coinciding with that of the initial laser radiation producing anisotropic photoelectrons. The minimum scale of the magnetic field corresponds to atomic dimensions.

Thus, the circular polarization of laser radiation is preferable for obtaining strong quasistationary magnetic fields compared to linear polarization. The Larmor gyration of electrons in a Weibel magnetic field does not disturb the Weibel effect, and only electron – electron collisions finally stop the development of instability of this type and limit the amplitude of the quasistatic Weibel magnetic field. Relativistic effects arise at comparatively low electron velocities and reduce the growth rate of the Weibel increment for a circularly polarized field, similarly to the case of linear polarization. This increment takes the maximum value at the relativistic intensity $I \approx 10^{19}$ W cm^{-2} of the laser field and equals half the value of the electron plasma frequency.

The Weibel instability mechanism in plasma is related to anisotropy of the electrons over the directions of their velocities. Such anisotropy arises in the process of ionization of atoms and atomic ions by superstrong laser fields. Most of the electrons escape along the direction of the electric field strength vector for a linearly polarized laser wave. The number of electrons escaping in transverse directions is significantly smaller. Both the longitudinal and transverse velocities are determined by the energy – time uncertainty relations. Weibel [84] was the first to show that the presence of electron current anisotropy in the Maxwell equations results in instability with respect to a spontaneous growth of the quasistatic magnetic field. The induction vector of this field is directed along the magnetic field induction of laser radiation. In the superstrong laser field, the characteristic time of instability growth is slightly above the reciprocal plasma frequency, i.e., is about several femtoseconds. Hence, the quasistatic magnetic field strengthens quite rapidly as compared to the duration of the laser pulse. The characteristic length over which this field varies amounts to dozens of angstroms. The field arises in the vicinity of the plasma critical surface. This mechanism is collisionless because collisions of electrons among themselves and with atomic ions level the electron velocity distribution, making it isotropic. Therefore, this mechanism can only be realized in a time lapse shorter than the characteristic time of electron collisions. First of all, electron – electron collisions should be considered. Indeed, in a superstrong laser field, electrons oscillate synchronously, following the electric field of a laser wave. Their velocity may be close to the speed of light, hence they hardly collide with atomic ions. Obviously, this oscillation component of the velocity is absent when electrons collide with each other due to the synchronous character of their oscillations. Thus, their relative velocity is rather low. The estimate of the induction of the magnetic field arising due to the Weibel instability has the simple form [83]

$$B \sim \frac{m\omega_{\rm pl}c}{e},$$

where $\omega_{\rm pl}$ is the plasma frequency, c is the speed of light, and m and e are the electron mass and elementary charge, respectively.

The thermoelectric mechanism, in contrast to the previous one, is realized in the collisional plasma, wherein gradients of both electron density and electron temperature exist and are directed at an angle to each other. The density gradient is directed along the radius of the electron beam. This gradient is caused by the inhomogeneity of laser radiation intensity over a focal spot. This results in the number of electrons on the axis of the laser beam being much greater than at the periphery due to the great difference in the degree of atomic ionization in the medium. Obviously, the temperature gradient has a normal direction to the target surface. The increment of growth for a spontaneous magnetic field is proportional to both the temperature and velocity gradients. The magnetic field in this case has toroidal symmetry: its annular field lines envelope the laser beam.

If the impinging laser pulse has relativistic intensity (the oscillating motion of electrons becomes relativistic, when the

laser radiation intensity is above 10^{18} W cm^{-2}), then plasma electrons are accelerated by the magnetic part of the Lorentz force along the direction of the laser pulse propagation. Here, we consider a plasma with a density below the critical value, so that the laser wave penetrates the plasma without noticeable attenuation. Such a plasma (in some cases it is called 'pre-plasma') is conventionally produced due to the effect of an unavoidable laser pre-pulse. The latter may be related to both small intensity peaks passing a few picoseconds ahead of the main laser pulse and a small pedestal at the leading edge of the main pulse. As a result, even in irradiating solid targets sufficiently rarefied plasma is produced with the plasma front moving towards the laser pulse. This plasma motion is similar to ambipolar diffusion, where heated electrons entrain heavy atomic ions in order to maintain the electrical neutrality of the ionized medium (the neutrality requirement is rather strong). The velocity of such motion is equal to the so-called velocity of plasma ion sound, which is determined by the thermal motion of atomic ions, albeit with the electron temperature. This velocity is usually on the order of 10^8 cm s^{-1}. But the pre-plasma expands to several micrometers in a matter of a picosecond. It is just this pre-plasma in which a superstrong quasistatic magnetic field is generated when the main laser pulse passes. This field is also toroidal, enveloping the lines of the electric current of electrons in the direction of the laser pulse propagation. It should be emphasized, however, that the magnetic part of the Lorentz force of the incident electromagnetic wave is not constant but oscillates (at a frequency twice that of the laser field, since the electron velocity and magnetic field induction comprised in the expression for the Lorentz force oscillate in opposite phases). That is why in such a simple situation electrons only oscillate along the direction of the laser pulse propagation at the double frequency. To obtain real drift of electrons, it is necessary to complicate the picture of motion. In the relativistic case, electrons in the electromagnetic wave field move along a trajectory which looks like a figure 8. The axis of the figure of eight is directed along the linearly polarized electric field vector, so that the laser pulse propagates in the normal direction to this axis (there is no motion along the magnetic field; recall that the electric field vector, the magnetic field vector, and the direction of wave propagation are perpendicular to each other). In passing one period of the incident wave, an electron does not return to the previous position on the figure eight trajectory, it slightly deflects from it. Just this effect causes drift of electrons in the direction of the laser pulse propagation. The nonadiabaticity of the drift process is caused by the production of electrons in the process of ionization of target atoms and atomic ions in pre-plasma. In the case of superstrong femtosecond laser pulses, a substantial part of the plasma electrons participate in such relativistic drift. Typical quasistatic annular magnetic fields generated in such a drift process in a underdense pre-plasma are on the order of 10 MG in intensity.

In Ref. [86], a magnetic field generated when intensive laser pulses propagate through a underdense plasma was measured. It is shown that at a duration of 30 fs and intensity of 4.2×10^{18} W cm^{-2}, the linearly polarized laser pulse produces an azimuthal magnetic field with the induction varying from 2 to 8 MG on a scale of about 200 μm. In the case of a circularly polarized laser pulse with a duration of 1 ps and intensity of 8×10^{18} W cm^{-2}, a solenoidal magnetic field was observed with an induction of about 7 MG, which corresponds to the inverse Faraday effect. Both magnetic

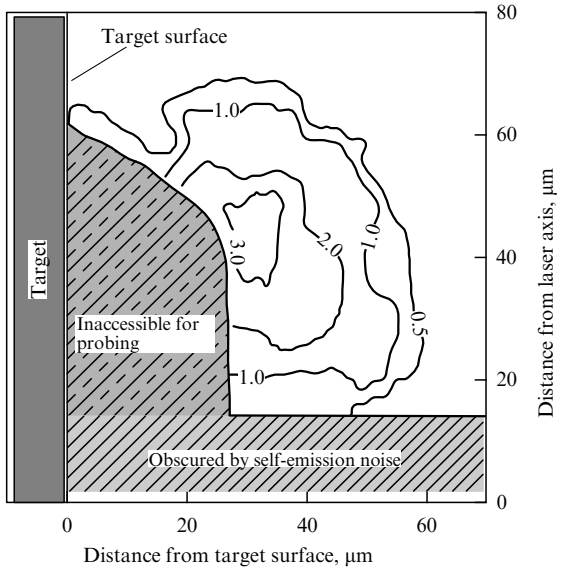

Figure 14. Topology of the magnetic field generated during the action of the picosecond laser pulse possessing the intensity of 5×10^{18} W cm^{-2} on aluminium foil 25 μm in thickness.

fields existed for several picoseconds. Their origin is ascribed to the jets of fast electrons arising in laser plasma.

Quasistatic magnetic fields were first measured in 1997 by the Faraday rotation of a test laser signal at moderate radiation intensities of 5×10^{18} W cm^{-2} [75]. The topology of the magnetic field was determined, which corresponded to the toroidal geometry with the axis directed along the laser beam. The spatial distribution of the magnetic field (in units of MG) is depicted in Fig. 14. Darkened regions in this figure correspond to the areas where measurements by this method cannot be performed. The temporal evolution of the maximum magnetic field intensity is presented in Fig. 15. One can see that the magnetic field is maintained for a time lapse an order of magnitude longer than the laser pulse duration. However, the reflection of the test radiation from density gradients is a serious limitation of this method and prevents one from measuring magnetic fields in the areas of the laser plasma wherein these fields are maximal. Propagation of a test signal is only possible in the areas possessing low plasma density, in which the magnetic field intensities are below 1–5 MG.

A numerical simulation [77] of the action of a laser pulse with a duration of 100 fs and intensity of 10^{19} W cm^{-2} in an overdense plasma of a solid target yielded the quasistatic magnetic field induction equal to ≈ 250 MG.

For measuring magnetic fields at higher radiation intensities of $(5-9) \times 10^{19}$ W cm^{-2} in overdense plasma [1, 87], an original method was applied based on propagation properties of the electromagnetic wave in magnetoactive plasma. These properties are related to the breakdown of the electromagnetic wave in magnetoactive plasma into ordinary and extraordinary modes, the latter being rather sensitive to the intensity and direction of the magnetic field in plasma. The third, fourth, and fifth harmonics generated in plasma were observed, and the cut-off points of the outgoing radiation were determined, which are uniquely related with the magnetic field induction. The measurements allow one to determine the range of intensities of the magnetic fields generated in dense plasma on the critical surface, which was found to be 340–460 MG

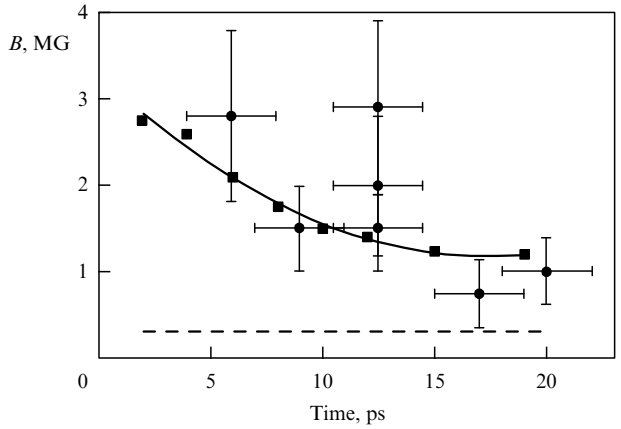

Figure 15. Temporal evolution of the maximum magnetic field induction registered in the experimental conditions corresponding to Fig. 14. The solid curve corresponds to MHD simulations, and the dashed curve corresponds to the sensitivity of the diagnostics at hand.

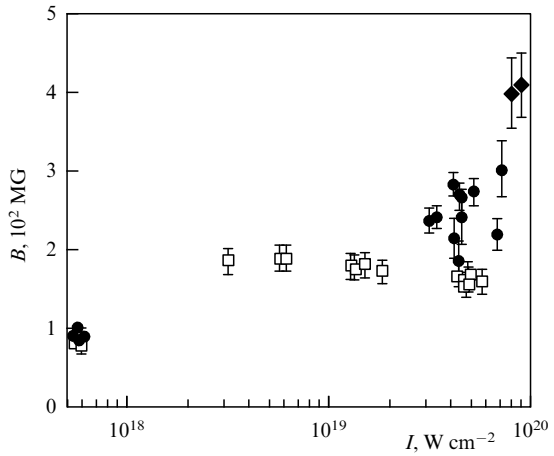

Figure 16. Measured magnetic field induction versus the intensity of laser radiation [1] for $5\omega(\blacklozenge)$, $4\omega(\bullet)$, and $3\omega(\square)$ harmonics.

(see Fig. 16). The magnetic pressure of such fields is above 10^9 atm.

The measurement data are in good agreement with particle-in-cell numerical simulations. The calculations modelled the interaction of a laser pulse with an initially plane target for an angle of the laser beam incidence of 45° relative to the target surface. The rise time and fall time of the laser pulse corresponded to four periods of the laser wave (12 fs), whereas the central part of the pulse comprised 24 periods of the laser wave (72 fs). It should be noted that the quasistatic magnetic field measured is only an order of magnitude weaker than the oscillating magnetic field of the laser pulse. A drawback of the numerical simulation was that it neglected electron – ion collisions, so that ions were kept cold.

In paper [88], the results of experiments on the irradiation of solid targets with a laser pulse with an intensity of about 10^{20} W cm^{-2} were presented. From optical polarization measurements of output harmonics (up to 15th) it was found that magnetic fields with an induction on the order of 700 MG arise in laser plasma. These magnetic fields are also present in the areas far exceeding a skin layer. This fact is explained by the ultrarelativistic motion of electrons in such strong laser fields and by the deep penetration of high harmonics of laser radiation into the target material. The ultrarelativistic depth of the skin layer can be obtained from the following approach [87]. Let us consider laser radiation with an electric field intensity E, which propagates along the z-axis. The relativistic Newton equation for electron motion along the x-axis of the polarization of laser radiation has the form

$$m\gamma \frac{\mathrm{d}v_x}{\mathrm{d}t} = m\gamma\left(\frac{\partial v_x}{\partial t} + v_z \frac{\partial v_x}{\partial z}\right) = -eE_x\,.$$

Here, γ is the relativistic factor for an electron. The second (convective) term on the left-hand side of this equation dominates the first term. Assuming $\partial/\partial z = 1/L$, where L is the relativistic depth of the skin layer, and $v_z \approx c$ (in the ultrarelativistic limit), one can rewrite the above equation in the form

$$m\gamma c \frac{v_x}{L} \sim eE_x\,.$$

From the Ampere law (rot $\mathbf{B} = 4\pi\mathbf{j}/c$) it follows that

$$\frac{B_y}{L} \sim \frac{4\pi e n_\mathrm{e} v_x}{c}\,.$$

In view of the previous equation we arrive at

$$B_y \sim \frac{4\pi e^2 n_\mathrm{e} L^2 E_x}{m\gamma c^2}\,.$$

From the Faraday law [rot $\mathbf{E} = -(1/c)\,\partial\mathbf{B}/\partial t$] it follows that

$$\frac{E_x}{L} \sim \frac{\omega B_y}{c}\,.$$

By excluding the electric and magnetic fields from the last two equations we find the ultrarelativistic depth of a skin layer [with allowance made for the definition of the nonrelativistic plasma frequency $\omega_\mathrm{pl}^2 = 4\pi n_\mathrm{e} e^2/m$]:

$$L = c\left(\frac{\gamma}{\omega_\mathrm{pl}^2 \omega}\right)^{1/3}\,.$$

This quantity is much greater than the nonrelativistic depth c/ω_pl of the skin layer.

The magnetic fields observed are also only an order of magnitude weaker than the oscillating magnetic field of the incident laser pulse.

A new method was suggested in work [89] for diagnosing giant magnetic fields in an expanding plasma which is produced by a petawatt laser pulse passing into solid targets. This method is based on the frequency shift of the radiation crossing the boundary of the expanding plasma. The harmonics of the incident laser pulse are used to analyze the plasma medium. The frequency shift strongly depends on the rate of plasma expansion; thus, in this way the rate can be measured. The frequency shift also depends on the polarization of harmonics. By observing the frequency shift for two orthogonal polarization states of photons propagating in a certain direction relative to the magnetic field, one can estimate the magnetic field inductions of up to 1 GG (provided the plasma frequency is known).

Laser plasmas, as opposed to current plasmas, are specific in the noticeably shorter pinching times which are too short for magnetohydrodynamic instabilities to develop (in the conditions of the experiment these instabilities are characterized by time increments on the order of 0.1 – 1 ns). This fact

may be rather important in further experiments with pinch structures, in particular, for realizing superdense compression of the substance as a result of 'radiative collapse', i.e., a reduction in the internal gas-kinetic pressure due to an intense radiation of the plasma compressed [90–99].

Recently, measurements of pinch effects in laser plasma were performed using the Vulcan setup [2]. Thin wire targets were irradiated with laser pulses with an intensity exceeding 5×10^{19} W cm^{-2}. The model of pinch origin suggests that a great number of relativistic electrons escape from the target, which results in the generation of strong reverse currents responsible for plasma pinching. The laser was focused on a spot 15 μm in diameter on the wire target. The diameter of the wires was about 20 μm, and the length was 3–5 mm. The character of pinch structures was detected by subjecting the target to a test laser pulse at double frequency, which was synchronized with the initial pulse. The rate of expansion and the dynamics of wire targets are surprisingly similar to the experiments with current pinches at currents ranging 100 kA – 1 MA.

Measurements of magnetic fields in plasma by various independent methods are very important for both proving the existence of such fields and determining their spatial structure (topology). For this purpose, we measured the profiles of X-ray spectral lines of hydrogen-like fluoride ions in laser plasma with a radiation intensity of 10^{17} W cm^{-2} and pulse duration of 1 ps [6]. The structure observed is characterized by distinct dips and peaks on the spectral line profiles (see Fig. 17). These features can be explained by invoking a conception of the strong turbulent noise that develops in the superstrong magnetic field generated in laser plasma.

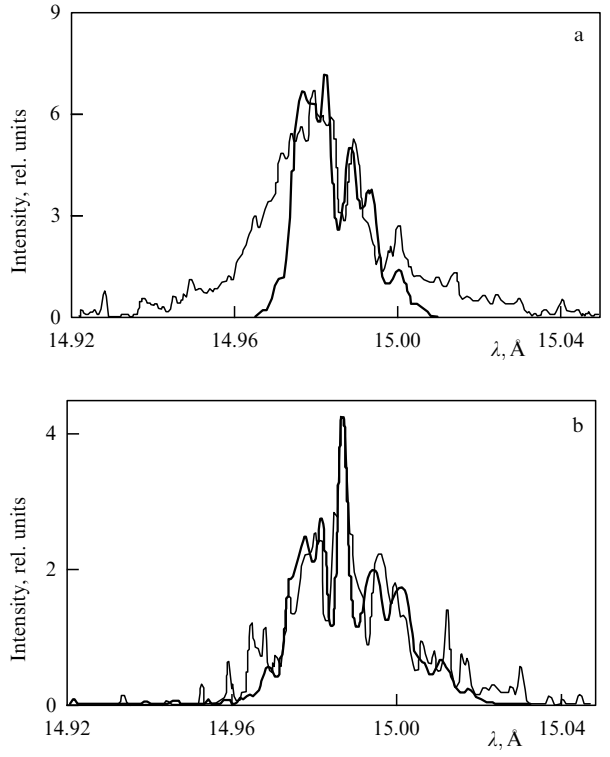

Figure 17. Comparison of experimental (thin curves) and theoretical (thick curves) profiles for the Ly_α line of F IX ion: (a) the experiment was performed at $I_{las} = 2 \times 10^{17}$ W cm^{-2}, and calculation was made at $T_i = 100$ eV, $n_e = 10^{20}$ cm^{-3}, $\omega = 7 \times 10^{14}$ s^{-1}, $E_0 = 4 \times 10^8$ V cm^{-1}; (b) the experimental $I_{las} = 3 \times 10^{17}$ W cm^{-2}, and the calculation was done at $T_i = 100$ eV, $n_e = 2 \times 10^{20}$ cm^{-3}, $\omega = 10^{15}$ s^{-1}, and $E_0 = 6 \times 10^8$ V cm^{-1}.

The static magnetic field arising under the action of laser pulses on plasma radically changes the character of the interaction between the laser pulse and the plasma medium. First and foremost, this is explained by resonances arising between the frequency of the laser radiation and the frequency of electron motion in the electromagnetic fields of the plasma. The main resonances of such a type are cyclotron and betatron resonances.

5. Conclusions

The above-described mechanisms for accelerating electrons and ions to a greater or lesser degree comply with up-to-date concepts on the generation of fast particles in laser plasma. According to these concepts, the energy of an initial laser pulse is converted to the energy of electron motion. The mechanisms for such energy conversion are mainly related to (1) a ponderomotive potential; (2) a phase interruption of electron oscillations in the laser wave due to various mechanisms, among which the main one is electron ejection beyond the sharp boundary of a target (vacuum heating), and (3) various resonance mechanisms where the electron motion is at resonance with plasma waves (wake-field resonance absorption or acceleration) or the cyclotron or betatron oscillation of an electron in the channel produced by laser radiation in the presence of a magnetic field. Ion acceleration in this case is a secondary effect mainly caused by the electric fields of the spatial charge produced when fast accelerated electrons are separated from ions. The detailed distribution of such fields substantially depends on the target thickness, which makes a difference in the ion acceleration at the front and rear target surfaces.

As a whole, particle acceleration is characterized by the multifactor character of the parameters involved. Such parameters are the intensity, frequency, and duration of the laser pulse; the contrast, which determines pre-plasma parameters; the thickness and structure of the target; the presence of magnetic fields, and some other factors. By combining these parameters, one can reach the optimal (in certain limits) conditions of particle acceleration. There is a wide range of various applications of such laser-driven accelerators, starting from fundamental investigations concerning nuclear processes for isotope production, to the initiation of thermonuclear reactions using laser setups that are quite small in size compared to standard accelerators, and ending by particular applications such as sources of proton radiation for medical purposes.

Nevertheless, there are a sufficiently large number of problems to be solved related to particle acceleration. These are, for example, ion beam focusing and annular structures arising in the beam. In electron acceleration, the problem of forming a monoenergetic beam of fast electrons with a maximum energy has not yet been solved.

As far as the generation of superstrong magnetic fields is concerned, the main problems are determination of their lifetime and topology. Experimental results definitely indicate that the lifetimes of magnetic fields are considerably longer (by orders of magnitude) than the laser pulse duration. From our point of view, this is direct evidence that long-living magnetic configurations exist in laser plasma. This is also confirmed by investigations into the dynamics of pinch

structures in irradiating wire targets by laser pulses. The topology and dynamics of such structures are, as was noted above, in surprisingly good agreement with those obtained under the pulse action of megaampere currents.

It is clear that the presence of high-intensity fast particles and magnetic fields in plasma, in addition to the specific features of particle acceleration mentioned above, should result in numerous instabilities arising in plasma. This is directly illustrated by the results mentioned above on measuring the profiles of spectral lines for multiply charged ions. Profile irregularity is indicative of the existence of intense electrostatic oscillations possessing definite frequencies and intensities. Thus, in view of all the specific features mentioned above, one can conclude that in the case of ultrashort laser pulses we are dealing with magnetoactive turbulent plasma, numerous properties of which are not clear presently. Nevertheless, it is possible to choose sufficiently optimal conditions for generating high-energy charged particles in such plasmas.

This work was supported by the International Science and Technology Center (project No. 2917) and the Russian Foundation for Basic Research (projects Nos 07-02-12060, 07-02-00080, 05-08-18167, and 08-02-00435).

References

1. Tatarakis M et al. *Phys. Plasmas* **9** 2244 (2002)
2. Beg F N et al. *Phys. Rev. Lett.* **92** 095001 (2004)
3. Umstadter D *J. Phys. D: Appl. Phys.* **36** R151 (2003)
4. Mourou G A, Tajima T, Bulanov S V *Rev. Mod. Phys.* **78** 309 (2006)
5. Andreev A V, Gordienko V M, Savel'ev-Trofimov A B *Kvantovaya Elektron.* **31** 941 (2001) [*Quantum Electron.* **31** 941 (2001)]
6. Belyaev V S et al. *Zh. Eksp. Teor. Fiz.* **126** 819 (2004) [*JETP* **99** 708 (2004)]
7. Belyaev V S et al. *Pis'ma Zh. Eksp. Teor. Fiz.* **81** 753 (2005) [*JETP Lett.* **81** 616 (2005)]
8. Brunel F *Phys. Rev. Lett.* **59** 52 (1987)
9. Wilks S C et al. *Phys. Rev. Lett.* **69** 1383 (1992)
10. Belyaev V S *Kvantovaya Elektron.* **34** 41 (2004) [*Quantum Electron.* **34** 41 (2004)]
11. Gus'kov S Yu et al. *Pis'ma Zh. Eksp. Teor. Fiz.* **73** 740 (2001) [*JETP Lett.* **73** 655 (2001)]
12. Demchenko N N, Rozanov V B *J. Russ. Laser Res.* **22** 228 (2001)
13. Pukhov A, Sheng Z-M, Meyer-ter-Vehn J *Phys. Plasmas* **6** 2847 (1999)
14. Esarey E et al. *IEEE Trans. Plasma Sci.* **24** 252 (1996)
15. Amiranoff F et al. *Phys. Rev. Lett.* **81** 995 (1998)
16. Pukhov A *Rep. Prog. Phys.* **66** 47 (2003)
17. Chen L M et al. *Phys. Plasmas* **8** 2925 (2001)
18. Cai H et al. *Phys. Plasmas* **13** 063108 (2006)
19. Bauer D, Mulser P *Phys. Plasmas* **14** 023301 (2007)
20. Rastunkov V S, Krainov V P *Laser Phys.* **15** 262 (2005)
21. Sentoku Y et al. *Appl. Phys. B* **74** 207 (2002)
22. Mangles S P D et al. *Phys. Rev. Lett.* **94** 245001 (2005)
23. Cai H et al. *Phys. Plasmas* **13** 113105 (2006)
24. Miyauchi K et al. *Phys. Plasmas* **11** 4878 (2004)
25. Singh K P *Phys. Plasmas* **11** 1164 (2004)
26. He F et al. *Phys. Rev. E* **68** 046407 (2004)
27. Kaplan A E, Pokrovsky A L *Phys. Rev. Lett.* **95** 053601 (2005)
28. Sazegari V, Mirzaie M, Shokri B *Phys. Plasmas* **13** 033102 (2006)
29. Startsev E A, McKinstrie C J *Phys. Plasmas* **10** 2552 (2003)
30. Kawata S et al. *Laser Part. Beams* **23** 61 (2005)
31. Korzhimanov A V et al. *Zh. Eksp. Teor. Fiz.* (2008)
32. Naumova N et al. *Phys. Rev. Lett.* **93** 195003 (2004)
33. Fedorov M V *Atomic and Free Electrons in a Strong Light Field* (Singapore: World Scientific, 1997)
34. Belyaev V S, Kostenko O F, Lisitsa V S *Pis'ma Zh. Eksp. Teor. Fiz.* **77** 784 (2003) [*JETP Lett.* **77** 653 (2003)]
35. Pavlenko Yu G *Lektsii po Teoreticheskoi Mekhanike* (Lectures on Theoretical Mechanics) (Moscow: Izd. MGU, 1991)
36. Tajima T, Dawson J M *Phys. Rev. Lett.* **43** 267 (1979)
37. Esarey E, Pilloff M *Phys. Plasmas* **2** 1432 (1995)
38. Malka V et al. *Phys. Plasmas* **8** 2605 (2001)
39. Thomas A G R et al. *Phys. Rev. Lett.* **98** 095004 (2007)
40. Mangles S P D et al. *Phys. Rev. Lett.* **96** 215001 (2006)
41. Gildenburg V B, Vvedenskii N V *Phys. Rev. Lett.* **98** 245002 (2007)
42. Pukhov A, Meyer-ter-Vehn J *Appl. Phys. B* **74** 355 (2002)
43. Yamagiwa M et al. *Laser Phys.* **16** 252 (2006)
44. Esirkepov T et al. *Phys. Rev. Lett.* **96** 014803 (2006)
45. Faure J et al. *Phys. Rev. Lett.* **95** 205003 (2005)
46. Kiselev S, Pukhov A, Kostyukov I *Phys. Rev. Lett.* **93** 135004 (2004)
47. Kando M et al. *Phys. Rev. E* **71** 015403(R) (2005)
48. Krasovitskii V B et al. *Phys. Plasmas* **11** 724 (2004)
49. Landau L D, Lifshitz E M *Elektrodinamika Sploshnykh Sred* (Electrodynamics of Continuous Media) (Moscow: Nauka, 1982) [Translated into English (Oxford: Pergamon Press, 1984)]
50. Sentoku Y et al. *Phys. Plasmas* **10** 2009 (2003)
51. Pukhov A *Phys. Rev. Lett.* **86** 3562 (2001)
52. Hatchett S P et al. *Phys. Plasmas* **7** 2076 (2000)
53. Krushelnick K, Clark E L, Zepf M *Phys. Plasmas* **7** 2055 (2000)
54. Maksimchuk A et al. *Phys. Rev. Lett.* **84** 4108 (2000)
55. Clark E L et al. *Phys. Rev. Lett.* **85** 1654 (2000)
56. Snavely R A et al. *Phys. Rev. Lett.* **85** 2945 (2000)
57. Wilks S C et al. *Phys. Plasmas* **8** 542 (2001)
58. Murakami Y et al. *Phys. Plasmas* **8** 4138 (2001)
59. Okihara S et al. *J. Nucl. Sci. Technol.* **39** 1 (2002)
60. Krainov V P, Smirnov B M, Smirnov M B *Usp. Fiz. Nauk* **177** 953 (2007) [*Phys. Usp.* **50** 907 (2007)]
61. Roth M et al. *Phys. Rev. ST Accel. Beams* **5** 061301 (2002)
62. Mackinnon A J et al. *Phys. Rev. Lett.* **86** 1769 (2001)
63. Mackinnon A J et al. *Phys. Rev. Lett.* **88** 215006 (2002)
64. Zepf M et al. *Phys. Rev. Lett.* **90** 064801 (2003)
65. Mora P *Phys. Rev. Lett.* **90** 185002 (2003)
66. Mora P *Phys. Rev. E* **72** 056401 (2005)
67. Fuchs J et al. *Nature Phys.* **2** 48 (2006)
68. Fuchs J et al. *Phys. Rev. Lett.* **94** 045004 (2005)
69. Kaluza M et al. *Phys. Rev. Lett.* **93** 045003 (2004)
70. Robson L et al. *Nature Phys.* **3** 58 (2007)
71. Cowan T E et al. *Phys. Rev. Lett.* **92** 204801 (2004)
72. Oishi Y et al. *Phys. Plasmas* **12** 073102 (2005)
73. d'Humières E et al. *Phys. Plasmas* **12** 062704 (2005)
74. Brantov A V, Bychenkov V Yu, Rozmus V *Kvantovaya Elektron.* **37** 863 (2007) [*Quantum Electron.* **37** 863 (2007)]
75. Borghesi M et al. *Phys. Rev. Lett.* **81** 112 (1998)
76. Stamper J A *Laser Part. Beams* **9** 841 (1991)
77. Wilks S C et al. *Phys. Rev. Lett.* **69** 1383 (1992)
78. Bell A R et al. *Phys. Rev. E* **48** 2087 (1993)
79. Bychenkov V Yu et al. *Pis'ma Zh. Eksp. Teor. Fiz.* **58** 183 (1993) [*JETP Lett.* **58** 184 (1993)]
80. Sudan R N *Phys. Rev. Lett.* **70** 3075 (1993)
81. Haines M G *Phys. Rev. Lett.* **78** 254 (1997)
82. Mason R J, Tabak M *Phys. Rev. Lett.* **80** 524 (1998)
83. Krainov V P *J. Phys. B: At. Mol. Opt. Phys.* **36** 3187 (2003)
84. Weibel E S *Phys. Rev. Lett.* **2** 83 (1959)
85. Krainov V P *Zh. Eksp. Teor. Fiz.* **123** 487 (2003) [*JETP* **96** 430 (2003)]
86. Najmudin Z et al. *AIP Conf. Proc.* **827** 53 (2006)
87. Tatarakis M et al. *Nature* **415** 280 (2002)
88. Wagner U et al. *Phys. Rev. E* **70** 026401 (2004)
89. Eliezer S et al. *Phys. Lett. A* **336** 390 (2005)
90. Gordeev A V, Loseva T V *Fiz. Plasmy* **29** 809 (2003) [*Plasma Phys. Rep.* **29** 748 (2003)]
91. Tzintsadze N L et al. *Phys. Plasmas* **9** 4270 (2002)
92. Sakagami Y et al. *Phys. Rev. Lett.* **42** 839 (1979)
93. Tatarakis M, in *Proc. of the 28th EPS Conf. on Controlled Fusion and Plasma Physics, 18–22 June 2001, Madeira, Portugal* (Ed. C Silva) (Madeira: Technopolo, Furchal, 2001)
94. Forslund D et al. *Phys. Fluids* **15** 1303 (1972)
95. Galeev A A et al. *Pis'ma Zh. Eksp. Teor. Fiz.* **15** 417 (1972) [*JETP Lett.* **15** 294 (1972)]
96. Bureeva L A, Gavrilenko V P, Lisitsa V S, in *Entsiklopediya Nizkotemperaturnoi Plazmy* (Encyclopedia of Low-Temperature Plasma) Vol. 1 (Ed.-in-Chief V E Fortov) (Moscow: Nauka, 2000)
97. Arefyev V I, Silin V P, Uryupin S A *Phys. Lett. A* **255** 307 (1999)
98. Tajima T, Kishimoto Y, Masaki T *Phys. Scripta* **T89** 45 (2001)
99. Lisitsa V S, Skovoroda A A *Eur. Phys. J. D* **38** 571 (2006)